European Journal of Pharmaceutical Sciences 212 (2025) 107204

Contents lists available at ScienceDirect

European Journal of Pharmaceutical Sciences

journal homepage: www.elsevier.com/locate/ejps

Transport across membrane meets biophysics to unveil the mechanism of action of a novel gH625 analogue

Rosa Bellavita [a,1], Annalisa Pecoraro [a,1], Sara Palladino [a], Camilla Danisi [a], Annarita Falanga [b], Gabriella D'Auria [a], Lucia Falcigno [a], Giulia Russo [a], Stefania Galdiero [a,*], Annapina Russo [a,*]

[a] Department of Pharmacy, School of Medicine, University of Naples Federico II, Via Domenico Montesano 49, 80131 Napoli, Italy
[b] Department of Agricultural Sciences, University of Naples Federico II, Via Università 100, Portici, 80055, Italy

ARTICLE INFO

Keywords:
Cell-penetrating peptide
Membrane interaction
In ovo toxicity

ABSTRACT

Cell-penetrating peptides are widely used in drug delivery for their ability to facilitate the transport of nanomaterials inside the cell. We previously studied the gH-625 for its ability to cross cell membranes, delivering various cargos into different cell types. In this study, since gH-625 suffers from low proteolytic stability, we identified the main cleavage sites after incubation with the enzyme chymotrypsin, and L-amino acids at these sites were replaced with their D-enantiomers, which share similar physicochemical properties but have distinct biological roles. Four peptides, namely gH-w10, gH-l7, gH-y13, and gH-combi, were designed and synthesized. Their biosafety profiles were evaluated in both normal and cancer cell lines and no significant toxic effects were revealed at the tested concentrations. Subsequently, we assessed their cell-penetrating ability by evaluating cellular uptake through fluorescence microscopy and investigated their mechanism of action in a model system of liposomes, measuring fusogenic activity, peptide insertion into the lipid bilayer, and leakage activity. The impact of the D-amino acid substitution on secondary structure was explored by circular dichroism and nuclear magnetic resonance studies. Finally, *in vitro* safety profiling data of the gH-625 and its most promising derivative gH-combi were further confirmed *in vivo* using a chicken embryo model.

1. Introduction

The membrane bilayer serves as a semi-permeable barrier that defines and protects the cell's interior, playing a crucial role in its survival and proper function (Sezgin et al., 2017; Cho et al., 2016). However, membrane complexity and limited permeability mean that only certain molecules can enter via active or passive transport, (Levental and Lyman, 2023; Klug et al., 2024) making effective intracellular delivery of many nanomaterials and anticancer drugs challenging (Kurrikoff et al., 2016; Kim et al., 2017; Fukuta and Kogure, 2022). While small molecules can diffuse through (Frallicciardi et al., 2022; Wu et al., 2024), larger one face solubility issues, restricting their pharmaceutical use (Yang and Hinner, 2015; Zhang et al., 2019). Developing efficient drug delivery systems is essential for precise targeting with minimal toxicity (Vargason et al., 2021; Kou et al., 2018; Liu et al., 2024). A key aspect of this is devising strategies to transport substances across membranes, a process that remains complex and not fully understood. Some peptides may offer a promising solution, as they might cross cellular membranes and other barriers such as the blood-brain barrier (BBB) (Wu et al., 2023; Zhou et al., 2021; Parrasia et al., 2022; Ghorai et al., 2023).

Cell-penetrating peptides (CPPs) are widely used in drug delivery both *in vitro* and *in vivo* due to their ability to safely transport materials into cells, (Gori et al., 2023; Voss et al., 2024) facilitating transmembrane movement of carriers and overcoming endosomal barriers (Zhang et al., 2023; Nikitovic et al., 2024). CPPs are generally biocompatible, non-toxic, and easy to synthesize and modify, making them valuable tools for drug delivery (Jafari et al., 2015; Bottens and Yamada, 2022; Moreno-Vargas and Prada-Gracia, 2024). These short peptides, typically rich in basic amino acids, are derived from proteins capable of crossing biological barriers, such as the viral TAT protein (Kalafatovic and Giralt, 2017; Brooks et al., 2005). Although the precise mechanism of CPP uptake remains under debate, it primarily involves the endocytic pathway, (Jiao et al., 2009; Ruseska and Zimmer, 2020)

* Corresponding authors.
E-mail addresses: sgaldier@unina.it (S. Galdiero), annapina.russo@unina.it (A. Russo).
[1] These two authors equally contributed to the work

https://doi.org/10.1016/j.ejps.2025.107204
Received 9 April 2025; Received in revised form 16 June 2025; Accepted 14 July 2025
Available online 15 July 2025

where the cargo is often trapped in endosomes (Walrant et al., 2017). This can result in degradation within lysosomes, reducing the efficiency of delivering therapeutic agents to their intended intracellular targets (Liu et al., 2024; Cleal et al., 2013; Mi et al., 2020; Dinca et al., 2016). Amphipathic peptides that effectively cross biological membranes can promote lipid membrane reorganizing processes which involve temporary destabilization and reorganization of the membrane (Hazrati and Vacha, 2024; Del Genio et al., 2022). These peptides can help overcome endosomal entrapment by either facilitating the escape of the cargo from endosomes or enabling its direct translocation across the plasma membrane into the cytosol (Dowaidar, 2024; Sahni et al., 2020).

A key advancement in understanding the role of amphipathic peptides is exemplified by the peptide gH-625 developed and widely studied by us (Galdiero et al., 2010). The peptide gH625, featured by the sequence HGLASTLTRWAHYNALIRAF, (Galdiero et al., 2010) has a membrane-disrupting domain containing crucial residues essential to interact and destabilize lipid membranes. gH625 is rich in hydrophobic amino acids such as glycine, leucine, alanine, and aromatic residues like tryptophan and tyrosine, which are typically positioned at the membrane interface (Galdiero et al., 2010). The peptide's interaction with lipids begins with its *C*-terminal arginine residue, in fact mutating this arginine significantly reduces its fusogenic activity. Biophysical studies on gH-625 have shown that it interacts with model membranes, penetrates the bilayer from its *N*-terminal side, and embeds its tryptophan residue within the membrane. It adopts a helical structure, with hydrophobic and aromatic residues aligned on one side of the helix and polar or charged residues on the other (Galdiero et al., 2012). Additionally, studies on peptides of varying lengths derived from gH-625 have revealed that their activity is influenced by both their sequence and length. Notably, the presence of a histidine residue at the *N*-terminus of the native gH625 sequence significantly boosts its fusion activity. This histidine facilitates the initial interaction with the membrane and promotes oligomerization (Galdiero et al., 2010). In its three-dimensional structure, both tryptophan and tyrosine are located on the same side of the helix, forming an amphiphilic structure (Galdiero et al., 2012). These residues play a crucial role in maintaining stability during membrane interaction. gH625 can deeply penetrate the lipid bilayer as an α-helix without causing major disturbances to the membrane, which may account for its ability to perform multiple functions. Its cellular uptake is linked to its hydrophobic and amphipathic properties, allowing it to interact with membrane lipids and form a transient helical structure that temporarily alters membrane organization, facilitating its insertion and translocation. Additionally, gH625 can traverse the blood-brain barrier (BBB), suggesting its potential as a nanocarrier for drug delivery to the central nervous system (Valiante et al., 2015; Barra et al., 2022).

This delivery ability of the peptide gH625 has been exploited by us for the construction of nanosystems able to deliver different cargos inside neuron cells or cancer cells (Valiante et al., 2015). In these studies, the nanosystems were decorated with gH625 on their surface and intracellular localization studies revealed their presence in cytosolic and perinuclear regions (Bellavita et al., 2024).

Although its remarkable characteristics, the peptide gH625 suffers from low proteolytic stability. Actually, various approaches, including cyclization strategies and substitution of L-amino acids with their D-enantiomers, are employed to address this issue (Pei et al., 2022; Li and Roller, 2002; Bellavita et al., 2023; Kremsmayr et al., 2022). Although D- and L-amino acids share similar physicochemical properties, their biological roles differ significantly (Lai et al., 2024). Replacing L-amino acids with D-amino acids can enhance resistance to enzymatic degradation, resulting in longer gastrointestinal, plasma, and intracellular half-lives (Zhao et al., 2016; Feng and Xu, 2016). These modifications could help protect the CPPs and extend their functional lifespan (Lucana et al., 2021; Al Musaimi et al., 2022; Yan et al., 2020).

In light of these considerations, herein, we measured the stability of gH625 in the presence of the enzyme chymotrypsin, and we designed and synthesized four gH625-analogues replacing L-amino acids involved in the cleavage site with their D-form. The effect on the delivery functionality of gH625 by D-amino acid replacement was explored by monitoring the internalization of novel derivatives in human keratinocytes and investigating their mechanism of action by biophysical characterizations. The biophysical studies were performed using eukaryotic model system as liposomes and the fusogenic activity, the peptide insertion inside the lipid bilayer, and leakage activity were measured. We also studied the effect of the D-amino acid replacement on the secondary structure performing circular dichroism both in solution and in liposomes mimicking eukaryotic membrane and nuclear magnetic resonance studies.

To evaluate the safety profile of gH625-analogues for drug delivery, their *in vitro* toxicity was tested on human keratinocytes (HaCaT), melanoma (A375), and colorectal cancer (RKO) cell lines. Given the limitations of *in vitro* models, (Lutolf et al., 2024) an *in ovo* toxicity test was also conducted using the chicken embryo model to assess gH625 and its most promising derivative, gH-combi.

Our results showed the possibility to use a more stable gH625 analogue for functionalizing nanomaterials and achieving drug delivery in theranostic applications of various human diseases.

2. Materials and methods

2.1. Materials

The N^{α}-Fmoc-protected conventional amino acids, Fmoc-His(Trt), Fmoc-Gly, Fmoc-Leu, Fmoc-Ala, Fmoc-Ser(tBu), Fmoc-Thr(tBu), Fmoc-Arg(Pbf), Fmoc-Trp(Boc), Fmoc-Tyr(tBu), Fmoc-Asn(Trt), Fmoc-Ile, and Fmoc-Phe were acquired from GL Biochem Ltd. (Shanghai, China). Fmoc-D-Leu, Fmoc-D-Tyr(tBu), Fmoc-D-Trp(Boc), Fmoc-rink amide resin, *N,N*-diisopropylethylamine (DIEA), piperidine, and trifluoroacetic acid (TFA) were purchased from Iris-Biotech GMBH. Oxyma pure, *N,N'*-Diisopropylcarbodiimide (DIC), 1-[Bis(dimethylamino) methylene]−1H-1,2,3-triazolo[4,5-b]pyridinium 3-oxid hexafluorophosphate (HATU), triisopropylsilane (TIS), Rhodamine B, acrylamide, 8-Aminonaphtalene-1,3,6-trisulfonic acid, disodium salt (ANTS), p-xylene-bis-pyridinium bromide (DPX), and human serum were acquired from Merck (Italy). Peptide synthesis solvents, *N,N*-dimethylformamide (DMF), diethyl ether (Et_2O), water, and acetonitrile (MeCN) for HPLC, were of reagent grade acquired from commercial sources (Merck and VWR) and used without further purification.

Phospholipids: Phosphatidylcholine (PC), Cholesterol (Chol), Rhodamine and 12-(N-methyl-N-(7-nitrobenz-2-oxa-1,3-diazol-4-yl)) (NBD)–phosphatidylethanolamine (Rho-PE and NBD-PE, respectively), were purchased from Avanti Polar Lipids (Birmingham, AL).

Cell cultures human epidermal keratinocytes (HaCat), melanoma (A375) and colorectal cancer (RKO) were acquired from American Type Culture Collection (ATCC) (Manassas, VA, USA).

Dulbecco's Modified Eagle Medium (DMEM), Fetal Bovine Serum (FBS), L-Glutamine, Penicillin-Streptomycin and Phosphate-Buffered Saline (PBS) were obtained from Gibco™ (Grand Island, NE, USA). 3-(4,5-dimethylthiazol-2-yl)-2,5-diphenyl tetrazolium bromide (MTT) and Propidium Iodide (PI) were purchased from Merck KGaA (Darmstadt, Germany).

Deuterium oxide (D_2O) of 99.9 % isotopic purity was purchased from Sigma Aldrich (Milan, Italy). Dodecylphosphorylcholine-d_{38} (DPC-d_{38}) of 98 % isotopic purity was purchased from Merck Life Science S.r.l. (Milan, Italy). Sodium-3-(trimethylsilyl) propionate 2,2,3,3-d_4 (TSP) was from Cambridge Isotope Laboratories (CIL), Inc. (Andover, MA, USA).

2.2. Peptide synthesis

All peptides were synthesized by embracing the solid-phase synthesis along with Fmoc/*t*Bu strategy (Barra et al., 2022). The resin Fmoc-Rink

amide (loading 0.67 mmol/g) was used as solid support. After the Fmoc deprotection from the resin by two treatments with a solution of 20 % piperidine for 10 min, the first amino acid Fmoc-Phe (2 equiv) was coupled performing two cycles: 1st coupling with DIC (2 equiv), Oxyma pure (2 equiv) in DMF for 25 min; 2nd coupling with HATU (2 equiv), DIPEA (4 equiv) in DMF, for 25 min (Barra et al., 2022). After the synthesis of the entire sequence, each peptide was cleaved from the resin simultaneously with the protecting groups on side chain amino acids by treating the resin with the strong acid solution TFA:TIS:H_2O (95:2.5:2.5, *v/v/v*) for 3 h at room temperature (Gesualdo et al., 2021).

Regarding Rhodamine labeled-peptides, before cleaving them from the resin, the Fmoc group from N-terminus was removed in basic conditions and then Rhodamin B (3 equiv) was added using HBTU (3 equiv), HOBt (3 equiv), DIPEA (6 equiv), in DMF, at overnight.

After the cleavage, each crude peptide was dissolved in MeCN 0.1 % TFA (10 %) and H_2O (0.1 % TFA), and purified by preparative high-performance liquid chromatography (HPLC) using Phenomenex Kinetex C18 column (5 μm, 100 Å, 150 × 21.2 mm) and linear gradients of MeCN (0.1 % TFA) in water (0.1 % TFA), from 10 to 90 % over 35 min, with a flow rate of 15 mL/min and UV detection at 220 nm. Their identity was confirmed by Electrospray Ionization Mass Spectrometry (ESI-MS) analysis and their pure profile was checked by analytical HPLC (Jasco LC-4000) (Figures S1-S10).

2.3. Peptide stability under chymotrypsin activity

The proteolytic stability of all gH-derived peptides was investigated incubating them with the enzyme chymotrypsin at the concentration of 0.01 μM (Vreeke et al., 2023). The peptide was dissolved in TRIS-HCl (100 mM, pH 7.8) buffer at the concentration of 200 μM and was incubated with the enzyme for 15, 30, and 60 min. At each time point, an aliquot of 50 μL was collected and the enzyme activity was quenched adding H_2O 0.2 % TFA. The proteolytic stability of gH625 and gH-combi was further investigated in the presence of 50 % human serum at different time intervals (15, 30, 60, 120, and 180 min) (Bellavita et al., 2023). An aliquot (50 μL) of the mixture was taken and MeCN was added to precipitate serum proteins; then, the mixture was cooled to 4 °C and centrifuged for 15 min (13,000 g rpm).

The proteolytic cut was analysed by HPLC using a Jupiter 4 u Proteo column, 90 Å, 150 × 4.6 mm) with a flow rate of 1 mL/min using a gradient of MeCN (0.1 % TFA) in water (0.1 % TFA) from 10 to 90 % over 20 min, and UV detection at 220 and 254 nm. The percentages were determined by integrating the chromatographic peak areas obtained from HPLC analysis and extrapolating the corresponding values using the calibration curve specific to each peptide. The peptide fragments derived from the cut of the peptide gH625 by chymotrypsin was identified by performing the ESI-MS analysis.

2.4. Cell cultures and treatments with gH625 and its analogues

Cell studies were carried out on HaCaT (human epidermal keratinocytes), A375 (melanoma) and RKO (colorectal cancer) were cultured as previously described (Lavecchia et al., 2013). Briefly, cells were cultured in Dulbecco's modified Eagle's medium (DMEM), supplemented with 10 % fetal bovine serum (FBS), 2 mM L-glutamine and 50 U/mL penicillin-streptomycin, under a humidified atmosphere of 5 % CO_2 at 37 °C. Treatments of cells were performed replacing the culture medium with those containing gH625 or its analogues at final concentration of 5 μM for cell uptake and from 1.25 to 40 μM for cytotoxicity assay.

2.5. Fluorescence microscopy

HaCaT cells were plated on coverslips at a density of 2×10^4 cells per well in 12-well plates and incubated with Rhodamine B-loaded peptides (5 μM). 2 h later, cells were analysed as previously described (Pecoraro et al., 2019). Briefly, cells were fixed with 3.7 % paraformaldehyde for 15 min. After washing, coverslips were mounted with PBS 1X-Glicerol (1:1) and stained with Hoechst nuclear staining to visualize the nuclei. Images have been acquired by using the Zeiss Cell Observer system composed by a motorized inverted microscope (Axiovert 200 M) and a digital camera (Axiocam H/R).

2.6. Cell uptake

The uptake of peptides in HaCat cells was evaluated on Rhodamine-loaded peptides (5 μM) by measuring the concentration of the fluorescent probe Rhodamine as previously described (Conte et al., 2023). Briefly, cells (1.5×10^4 cells per well in 24-well plates) were collected and analysed by fluorimetry on a Cary Eclipse fluorescence spectrophotometer (Varian). Each peptide at 5 μM was added and incubated for 2 h to monitor the cellular internalization. A calibration curve of each Rhodamine B-labeled peptide in the medium was built at the concentration of 5 μM. Excitation and emission wavelengths were 546 and 568 nm, respectively. Statistical comparisons were made as previously shown (De Filippis et al., 2014).

2.7. Structural studies

The secondary structure of all peptides was studied by Circular Dichroism (CD) spectroscopy. The structural studies were performed in solution and in liposomes mimicking eukaryotic membranes. Each peptide was dissolved in water at 50 μM and CD spectrum was recorded from 195 to 260 nm using a Jasco J-1500 CD Spectrometer with a quartz cell (0.1 cm) at room temperature. Each spectrum was obtained by averaging three scans and converting the signal to molar ellipticity. In membrane environment, SUVs at the concentration of 100 μM was prepared as described above and the peptide was added at the ratio peptide/lipide of 1 and 1.5. CD spectra were recorded from 190 to 260 nm with a quartz cell 0.1 cm and converting the signal to molar ellipticity.

2.8. NMR spectroscopy

An appropriate amount of peptide was dissolved in 0.600 mL H_2O/D_2O 90/10 (*v/v*) for a peptide concentration of 0.5 mM to carry out the NMR analysis in pure water. Then, increasing volumes (μL) of a stock DPC-d_{38} solution (1.0 M in H_2O/D_2O 90/10 *v/v*, pH 6) were added until no modification was observed on the one-dimensional spectra. The NMR analysis in micellar environments was performed at DPC/peptide molar ratio R of 100, corresponding to DPC concentrations of 50 mM and peptide concentration of 0.5 mM. NMR spectra were recorded on Bruker 600 and 700 MHz Spectrometers, located at the Department of Pharmacy – University "Federico II" of Naples, and equipped with a z-gradient 5 mm triple-resonance cryoprobe. One-dimensional proton (1D) and two-dimensional homonuclear (2D) NMR spectra were recorded at a temperature of 298 K. The spectra were calibrated relative to TSP (0.00 ppm) as an internal standard. 2D TOCSY (mixing times 70 ms), and NOESY (mixing times 300 ms) spectra were recorded in the phase-sensitive mode using the method from States, using 4096 data points in t2 and 512 equidistant t1 values. The water resonance was suppressed by use of gradients. 1D NMR spectra were analysed by MESTRENOVA 6.0 software (Mestrelab Research, S.L, Santiago de Compostela, Spain) and 2D NMR spectra by CARA program ((http://cara.nmr.ch/doku.php/home). Proton resonances were sequentially assigned by following the Wuthrich standard method (Wuthrich, 1986). The molecular models were visually analyzed by PyMOL software Molecular Graphics System, Version 2.0 Schrödinger, LLC (DeLano (2002) http://www.pymol.org).

2.9. Lipid mixing and leakage assays

Lipid mixing experiment was performed by exploiting the resonance energy transfer assay using the NBD Rho as donor and acceptor probes, respectively (Struck et al., 1981). We prepared LUVs made of PC:Chol 1:1 at the concentration of 0.16 mM and LUVs made of PC:Chol with 0.6 % mol of NBD-PE and 0.6 % mol of Rho-PE at the concentration of 0.04 mM. For the evaluation of membrane mixing, unlabelled and labelled LUVs were mixed at a 4:1 ratio to have final lipid concentration of 0.1 mM (Galdiero et al., 2008). In the experiment, each peptide was added to LUVs at increasing concentrations in according to lipide/peptide ratio of 0.01, 0.02, 0.03, 0.05, 0.1. The lipid mixing was evaluated by recording the NBD emission at 530 nm and Rho emission at 590 nm followed with the NBD excitation wavelength set at 465 nm. The percentage of fusion after each peptide addition was calculated as a function of 100 % value corresponding to complete mixing of all lipids upon the addition of Triton X-100 (0.05 % *v/v*). The percentage fusion was calculated as:

$$\frac{[F530/F590]peptide - [F530/F590]blank}{[F530/F590]triton - [F530/F590]blank} \; x\; 100$$

where F530 and F590 are the fluorescence intensities at 530 nm and 590 nm calculated in the absence and in the presence of the peptide and Triton X-100.

In addition, lipid mixing of the inner monolayer was measured by a modification of the phospholipid-mixing measurement (Cummings and Vanderlick, 2007). LUVs made of PC:Chol (0.04 mM) with 0.6 % mol of NBD-PE and 0.6 % mol of Rho-PE were prepared and treated with sodium dithionite dequenching NBD-labeled phospholipid located at the outer monolayer of the membrane (Falanga et al., 2011). Sodium dithionite was dissolved in buffer TRIS 1 M pH 10, added to LUVs at the concentration of 100 mM and incubated for 1 h on ice in the dark. The excess of sodium dithionite was removed by performing size exclusion chromatography through a Sephadex G-75 filtration column using as eluent the buffer 10 mM TRIS, 100 mM NaCl, and 1 mM EDTA, pH 7.4. Then, labelled LUVs were mixed with unlabelled and LUVs at a 1:4 ratio at final lipid concentration of 0.1 mM. The inner monolayer fusion was evaluated recording NBD emission at 530 nm after addition of increasing peptide concentrations to LUVs in according to lipide/peptide ratio of 0.01, 0.02, 0.03, 0.05, 0.1. The percentage of inner monolayer fusion was calculated as described above.

Regarding the peptide ability to induce the leakage liposomes, we performed the ANTS/DPX leakage assay by preparing LUVs with encapsulated ANTS and DPX (Aguilera et al., 2021; Wimley, 2015). The lipid film was prepared as described above and before the lyophilization ANTS (12.5 mM) and DPX (45 mM) dissolved in water were added (Bellavita et al., 2023). After the lyophilization, the lipid-probes film hydrated with PBS 1 × buffer, vortexed for 1 h and treated to obtain LUVs as described previously. Then, LUVs were treated to remove the excess of probes performing the gel filtration using a Sephadex G-50 column (1.5 cm × 10 cm). The liposome leakage was evaluated treating LUVs with increasing concentrations of each peptide (1, 3, 5, 10, 15, 20, 30, and 50 μM) and spectra were recorded exciting ANTS at 385 nm (slit width, 5 nm) and measuring ANTS fluorescence emission at 512 nm (slit width, 5 nm). The data were normalized in according to the complete ANTS release obtaining treating LUVs with 0.1 % Triton X which causes the total liposome leakage. The percentage of leakage was calculated as % leakage = $(F_i–F_0)/(F_t–F_0)$, where F_0 represents the fluorescence of intact LUVs before the addition of peptide, while F_i and F_t denote the intensities of the fluorescence achieved after peptide and Triton-X treatment, respectively.

2.10. Membrane integrity assay

HaCaT cells were seeded in 24-well plates and cultured for 24 h prior to treatment with 5 μM of gH625 and gH-combi. Subsequently, PI (4 μg/ml) was added to the cells, which were incubated for 30 min at 37 °C while protected from light. After incubation, the cells were examined using a fluorescence microscope to assess membrane integrity based on PI fluorescence uptake.

2.11. Tryptophan quenching in solution and large unilamellar vesicles (LUVs)

The insertion of each peptide was studied in buffer and in large unilamellar vesicles (LUVs) performing the quenching of tryptophan (Trp) located in position 10 using the quencher acrylamide at different concentrations (Mukherjee et al., 2024; Strambini and Gonnelli, 2010). In HEPES buffer, each peptide at the concentration of 10 μM was quenched with increasing concentrations of acrylamide from 0.02 M to 0.22 M. For the quenching in membrane environment, LUVs composed of phosphatidylcholine (PC) and cholesterol (Chol) at the ratio 1:1 was used to mimic eukaryotic membrane. LUVs were prepared according to extrusion method as reported elsewhere (Bellavita et al., 2023). Firstly, the stock solutions of phospholipids were prepared by dissolving them in chloroform and then the right amount was taken from each solution for the formation of lipid film PC:Chol 1:1 at the final concentration of 250 μM. The lipid film was hydrated with HEPES buffer, vortexed for 1 h at room temperature, and then was freeze-thawed 6 times and extruded 10 times through polycarbonate membranes with 0.1 μm diameter pores to obtain LUVs. For monitoring the Trp insertion in LUVs, each peptide at the concentration of 10 μM was incubated with liposomes and the acrylamide was added at the concentrations ranging from 0.02 M to 0.22 M to quench Trp fluorescence. Each Trp spectrum was recorded setting the fluorescence excitation at 295 nm. The data in solution and in LUVs were analysed with the Stern-Volmer equation, $F_0/F = 1+Ksv[Q]$, where F_0 and F indicate the fluorescence intensities in the absence and the presence of the quencher (Q), respectively; while Ksv is the Stern-Volmer quenching constant, which is correlated to the accessibility of Trp residue to acrylamide.

The quenching experiment was also performed with the phospholipids labelled with bromo probe that is a Trp quencher (Bolen and Holloway, 1990). LUVs were prepared containing 25 % of phospholipids bearing bromo in different positions; specifically we used 1-palmitoyl-2–(4,5-dibromo)s-tearoyl-sn-glycero-3-phosphocholine (4,5 Br-PC) and 1-palmitoyl-2–(11,12-dibromo)stearoyl-sn-glycero-3-phosphocholine (11,12 Br-PC). After the preparation of LUVs composed of PC:PC-Br:Chol (ratio 0.25:0.25:0.5), each peptide was incubated with LUVs and the Trp spectrum was recorded.

2.12. Chymotrypsin proteolytic cut by fluorescence assay

The insertion of Trp was further monitored in the presence of the enzyme chymotrypsin both in buffer and small unilamellar vesicles (SUVs) made of PC:Chol 1:1. The chymotrypsin has high affinity for hydrophobic amino acids and when it cuts the bound involving Trp residue induces an increase of Trp fluorescence (Ma et al., 2005). The experiment was performed dissolving the peptide at 5 μM in buffer (TRIS-HCl 100 mM pH 7.3) and then was incubated with chymotrypsin (1 μM). The fluorescence intensity was recorded with λ_{ex} 295 nm and λ_{em} 355 nm within 15 min corresponding to the Trp fluorescence (Galdiero et al., 2010). Each Trp spectrum was recorded in solution and upon the addition of the enzyme. The same experiment was performed in SUVs using a ratio lipide/peptide of 3000. SUVs were prepared hydrating the lipid film with the TRIS-HCl buffer, vortexed for 1 h, freeze-thawed 6 times and sonicated for 40 min. The peptide at 5 μM was incubated with SUVs for 10 min and then was incubated with chymotrypsin. The Trp fluorescence intensity was recorded with λ_{ex} 295 nm and λ_{em} 355 nm within 15 min.

2.13. Cytotoxicity assay

Cells were seeded onto 96-well plates (1×10^4 cells/well) and incubated with all peptides (from 1.25 to 40 μM) for 24 h. Then, cell viability was evaluated by the 3-(4,5-dimethylthiazol-2-yl)-2,5-diphenyl-2H-tetrazolium bromide (MTT) as previously reported (Virgilio et al., 2021). The absorbance was measured at 570 nm using a microplate reader (Biotek Synergy H1 Hybrid multiplate reader). Then, cell viability was calculated respect to control cells and expressed as percentage.

2.14. In ovo toxicity test

Fertilized chicken eggs were obtained from a commercial certificated hatchery, stored in a refrigerator (10 °C) for 1–3 days and then incubated as previously (Brignola et al., 2024). The first day of incubation was considered as egg development day (EDD) zero (EDD0). On EDD3, eggs were stored vertically 30 min before sample injection. Sterilized 1 mL syringe with needle was used to create a hole through the eggshell and to inject 100 μL of the sample into albumen. Eggs were randomly allocated into four groups ($n = 15$ eggs per group). The first and second groups were treated with gH625 and gH-combi, respectively. The third group received toluene as positive control, and the fourth group was negative control, which receive 100 μL of vehicle (sterile H_2O Milli-Q). To avoid contamination, all injections were performed in a clean room and all the equipment were sterilized. The injection site was sealed with sterile surgical adhesive tape and the eggs were returned into the hatchery. Chicken embryo viability and development were assessed on EDD8, 12 and 16. To isolate liver and heart on EDD16, each embryo was decanted from the cut shell and transferred to a clean Petri dish breast side up. Then, the embryo was washed several times with PBS and transferred to another fresh Petri dish containing PBS. The embryo was dissected by cutting through the sternum, and the internal organs were subsequently removed.

3. Results and discussions

3.1. Peptide design and synthesis

Deep biophysical and biological studies focused on the mechanism of action demonstrated the strong capability of gH-625 to interact and diffuse across the cell membrane not causing leakage through pore formation, but mainly using a translocation mechanism which induces a temporary and local membrane destabilization and consequent reorganization (Galdiero et al., 2010; Falanga et al., 2011). Despite the peptide gH625 represents a high promise in intracellular delivery and is able to cross the cell membrane in a short time, (Valiante et al., 2015; Bellavita et al., 2024) it is easily recognized and degraded by proteases for its chemical nature causing a reduction of its intracellular half-live. Hence, to overcome this main obstacle without influencing its cell-penetrating capacity, we studied the proteolytic cut of gH625 in presence of the enzyme chymotrypsin to identify the main cleavage sites and to design its enhanced version.

Firstly, the peptide gH625 was incubated with the enzyme chymotrypsin (0.01 μM) at different time points including 0, 15, 30 and 60 min. As we expected, the peptide was rapidly recognized by chymotrypsin, in fact, we detected ~50 % and ~10 % of the intact peptide after 15 and 30 min, respectively. Thus, to design an enhanced version of gH625, the most abundant degraded products were identified by performing high performance liquid chromatography (HPLC) and electrospray ionization mass spectrometry (ESI-MS) analysis. Since the enzyme chymotrypsin has a large preference towards aromatic and hydrophobic amino acids, (Vreeke et al., 2023) tryptophan (W), leucine (L), and tyrosine (Y) could be major residues involved in the cleavage of gH625. Indeed, through an analysis of the most abundant fragments a_1–a_5 reported in the Fig. 1 (also see supporting information, Figure S11), we recognized three main cleavage sites involving specifically the peptide bound between: *i)* L^7 and T^8; *ii)* W^{10} and A^{11}; *iii)* Y^{13} and N^{14}.

Aiming to extend the protection to chymotrypsin, L-hydrophobic amino acids involved in the peptide hydrolysis were replaced with their D-enantiomeric form because the D-form presents different side-chain orientation and less affinity toward the enzyme. This strategy could enhance outstanding resistance to proteolytic degradation modifying peptide backbone but not causing a reduction of peptide efficiency and affinity. Thus, in our design, we replaced the residues L^7, W^{10} and Y^{13} with their D-enantiomeric form synthesizing three gH-625 analogues, gH-w10, gH-l7, and gH-y13, reported in Table 1. In addition, we also synthesized the combination form of gH-625 in which three residues L^7, W^{10} and Y^{13} were simultaneously replaced with their D-enantiomers obtaining the peptide gH-combi.

All peptides were synthesized using the solid-phase peptide synthesis combined with Fmoc/*t*Bu strategy. The resin Rink amide was used to achieve the C-amidated peptide. A basic solution of 20 % piperidine in DMF was used for Fmoc deprotection, while coupling reactions were carried out by two different cycles: 1st cycle with DIC (2 equiv), Oxyma pure (2 equiv) in DMF; 2nd cycle with HATU (2 equiv), DIPEA (4 equiv) in DMF. After the complete synthesis and the cleavage, each peptide was purified by HPLC, and identity was confirmed by ESI-MS analysis. All the purified peptides were obtained with good yields (approximatively 40 %).

Table 1
Peptide sequence of gH-625 analogues designed and synthesized in this study.

Peptide	Sequence
gH625	HGLASTLTRWAHYNALIRAF
gH-dl7	HGLAST*l*TRWAHYNALIRAF
gH-dw10	HGLASTLTR*w*AHYNALIRAF
gH-dy13	HGLASTLTRWAH*y*NALIRAF
gH-combi	HGLAST*l*TR*w*AH*y*NALIRAF

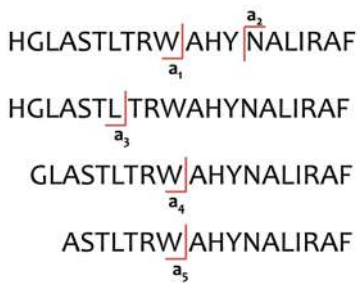

Fragment	Sequence	Mass found
a_1	HGLASTLTRW	[M+H⁺]=1141.7 [M+2H⁺]/2= 571.7
a_2	NALIRAF	[M+H⁺]=803.6 [M+2H⁺]/2= 402.6
a_3	HGLASTL	[M+H⁺]=698.5
a_4	GLASTLTRW	[M+H⁺]=1033.7 [M+2H⁺]/2= 515.3
a_5	ASTLTRW	[M+H⁺]=833.5 [M+2H⁺]/2= 417.5

Fig. 1. The fragmentation of the peptide gH-625 by the enzyme chymotrypsin and the peptide fragments identified by ESI-MS analysis.

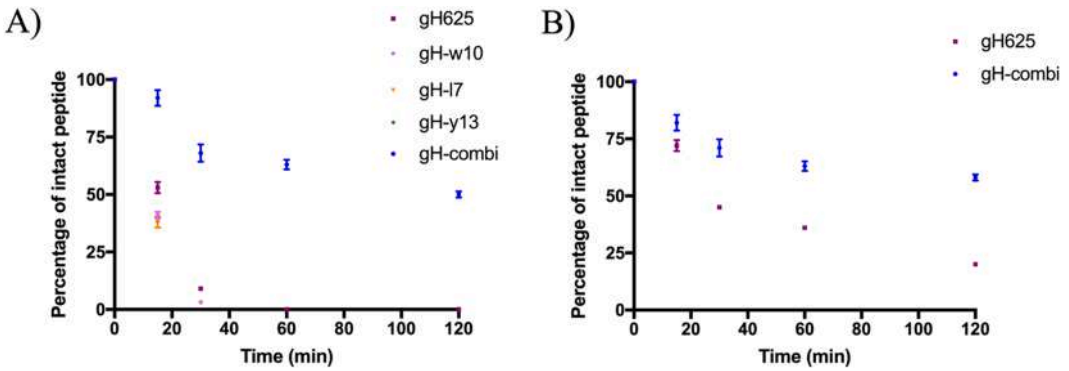

Fig. 2. Panel A: The percentage of the intact peptide after the incubation with chymotrypsin (0.01 μM) at 15, 30, 60, and 120 min. Panel B: The percentage of the intact peptide after the incubation with human serum (50 %) at 15, 30, 60, and 120 min. The percentages were determined by integrating the chromatographic peak areas obtained from HPLC analysis. Data represent the mean ± SD of three independent experiments.

3.2. Peptide stability

The stability of each peptide was measured in the presence of the chymotrypsin (0.01 μM) at 37 °C and at different time points (0, 15, 30, 60, and 120 min). The percentage of the intact peptide was calculated by integrating the peak area of the chromatogram from the HPLC analysis.

As observed in Fig. 2, the peptides gH-l7, gH-w10, and gH-y13 have a similar trend to the native peptide gH625, while the combination version gH-combi successfully showed an increase of the resistance toward the chymotrypsin. In fact, the peptides gH-w10, gH-l7, and gH-y13 were fully degraded after 60 min of the incubation, detecting just ~50 % of the intact form already after 15 min. In contrast, the combination form including three D-amino acids induced an improved resistance to the proteolytic cut because the peptide gH-combi was still present (~50 %) after 120 min.

Therefore, the incorporation of amino acids D-Leu, D-Trp, and D-Tyr allowed to achieve an enhanced version of gH-625, but since our aim was to make gH625 more stable without losing its delivery capability, the influence of this chemical approach on its functionality was evaluated *in vitro* through the cellular internalization into living cells and several biophysical studies.

Additionally, we evaluated the stability of the peptide gH-combi in 50 % human serum, using the reference peptide gH625 for comparison. Both peptides were incubated with serum for 15, 30, 60, and 120 min. At each time point, an aliquot of the mixture was collected, and proteins were precipitated using MeCN. As shown in Fig. 2 (panel B), gH625 underwent significant degradation over time, with only ~30 % of the peptide remaining after 120 min. In contrast, gH-combi retained ~58 % of its intact form at the same time point. These findings support the effectiveness of our rational design strategy, demonstrating that the D-amino acid incorporation can significantly enhance the serum stability of the native peptide.

3.3. Internalization of gH625 and its analogues in HaCaT cell line

The impact of chemical modifications on the cell-penetrating ability of gH625 was investigated by evaluating the cellular uptake of its novel analogues using fluorescence microscopy. Each peptide was conjugated at the N-terminus with Rhodamine (Rho) as a fluorescent marker. The internalization of Rho-labeled peptides (5 μM) was assessed after 2 h of incubation with HaCaT cells at 37 °C. As shown in Fig. 3 (panel A), all peptides successfully entered the cells and localized to the cytoplasm, although their internalization efficiencies varied markedly. To quantitatively evaluate cellular uptake, spectrofluorometric analysis was performed. The results, shown in Fig. 3 (panel B), confirmed the microscopy observations and revealed varying internalization rates among the peptides. Specifically, the peptide gH-combi exhibited the highest uptake, with nearly 90 % internalization, while gH-y13 demonstrated 75 % internalization, similar to the native gH625 peptide. In contrast, gH-l7 and gH-w10 peptides displayed reduced cellular penetration relative to gH625.

3.4. Effect of D-amino acids incorporation on the conformation

The functionality of the peptide gH625, including its fusogenic activity and membrane crossing, depend on its structural conformation as demonstrated in our previous works (Galdiero et al., 2012). Specifically, gH625 adopts a random structure in solution, while forms a α-helical structure with an amphiphilic character in membrane-mimicking micellar environment. This helix conformation typical of fusion peptides is extremely crucial because it favors their insertion into the membrane and translocation. The impact of D-amino acid incorporation on the secondary structure was evaluated in water and using small unilamellar vesicles (SUVs) made of phosphatidylcholine (PC) and cholesterol (Chol) at the molar ratio 1:1. CD spectra reported in Fig. 4, were recorded at different peptide/lipid (P/L) ratios of 1 and 1.5.

All the peptides in solution adopted a typical random coil structure with a minimum close to 200 nm, except for the peptide gH-combi that presents two minimum at 200 nm and 228 nm. Regarding the peptide conformation in the membrane environment (PC:Chol, 1:1), the peptides gH-w10 and gH-l7 showed a random conformation even at the highest ratio P/L of 1.5, while gH625 and gH-y13 adopted the helical conformation in the presence of SUVs at the highest ratio P/L of 1.5. Instead, in the presence of SUVs, gH-combi changes its conformation and shows a shift of the minimum at 200 towards higher wavelengths and the presence of a non-canonical minimum at 228 nm, which is more intense compared to the spectrum in water. Our hypothesis is that the minimum at 228 is likely correlated to the presence of the two aromatic D-amino acids (w10 and y13) that when located in the same peptide may be involved in π-stacking interactions determining an atypical band and favoring the helical rearrangement especially in SUVs.

3.5. NMR analysis of gH-combi in aqueous and micellar environments

The conformation of the 20-residue gH-combi peptide was analysed via NMR both in water, where it is perfectly soluble, and in micelle environment by Dodecyl-phosphorylcholine (DPC). In pure water, the peptide is mainly unstructured, a diagnosis obtained both based on modest chemical shift deviations of the α CH protons from the random coil values (see cyan bars in Fig. 5) and for the absence of patterns of NOE effects expected in case of stable secondary structures (Wishart et al., 1991).

The ability of gH-combi to interact with micelles made up of DPC was probed via NMR in two ways: i) dissolving the peptide in a 50 mM DPC solution, ii) adding increasing quantities of stock micellar solution 1.0 M to the peptide in water, up to a DPC monomer/peptide ratio of 60. As

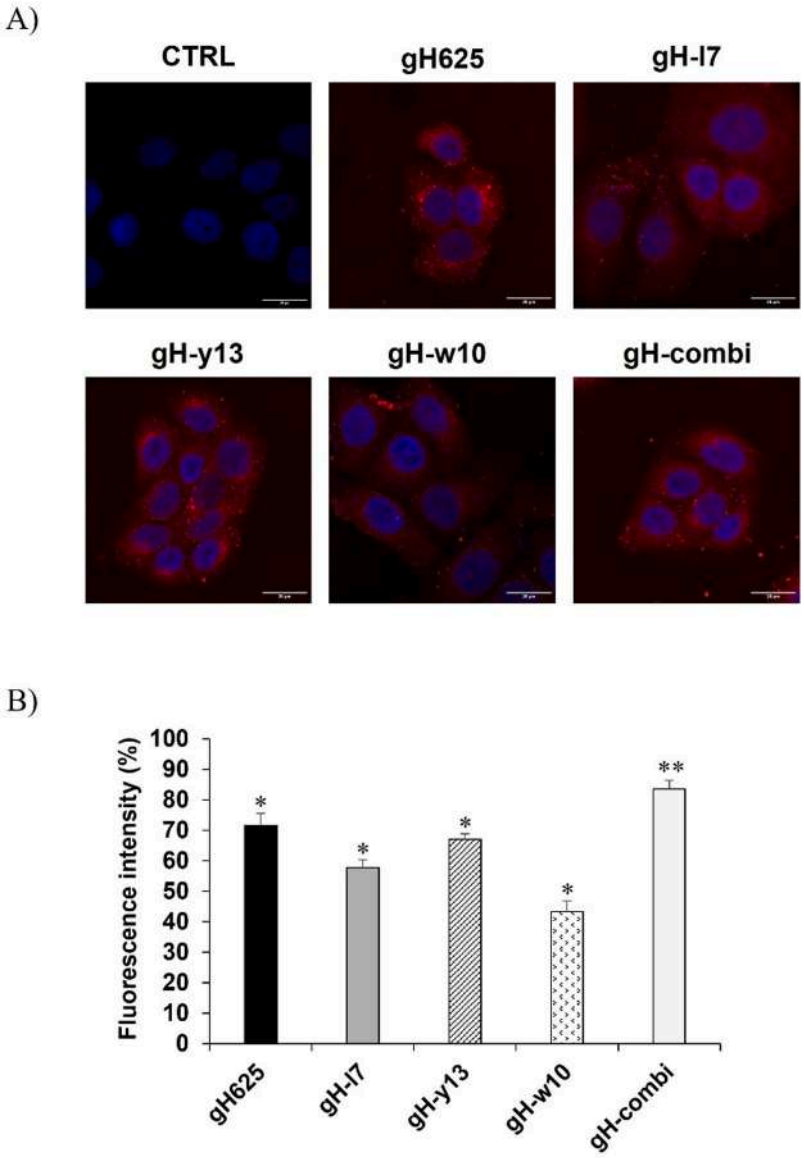

Fig. 3. Internalization of gH625 and its derivatives in HaCaT cells. (A) Representative fluorescent microscopy images of HaCat cells after 2 h of incubation with 5 μM of each peptide. The merged channels of Rhodamine-labeled peptides (red) and Hoechst-counterstained nuclei (blue) are reported. Bar size: 20 μM. (B) Spectrofluorimetric analysis of HaCat cell uptake after exposure to gH625 and its derivatives. Bars represent the mean of triplicate experiments; error bars represent the standard deviation. * $p < 0.05$; ** $p < 0.01$.

reported in Fig. 6, the spectra acquired at different ratios showed both a progressive line broadening and chemical shifts variation for numerous resonances. Both phenomena confirm, independently of each other, that gH-combi interacts with micelles. The broadening of the lines is in fact associated with an increase in the transversal relaxation rates of the protons (R2) which in turn are almost proportional to the molecular mass and the tumbling time. The translation of the peptide from the free form to that adherent to the micelles involves a change in the molecular tumbling times which is reflected in the reduction of R2 and in wider lines. On the other hand, the chemical shift changes that are observed as R ratio increases indicate that the peptide changes its conformational distribution, a phenomenon that occurs thanks to the change in the surrounding environment, from that of the solution to that of the surface and/or micellar interior.

The best condition for the structural characterization of the peptide in the presence of micelles was identified in the system with gH-combi peptide in a micellar environment 50 mM DPC/water. In such an environment, gH-combi adopts a distribution of conformations among which ordered structures can be identified. Spectral analysis allows the assignment of only one family of structures among the others. For this family, the negative αCH deviations from random coil values < -0.1 ppm (orange bars Fig. 5) point to a helical arrangement.[32] This structural diagnosis is consistent with the NOE effects observed in the NOESY spectrum. It is to note that some backbone αCH protons, particularly those belonging to the central region of peptide (from D-Leu^7 to Asn^{14}) show very poor intensities, suggesting that this region could be in deep interaction with the micelles.

These effects make challenging to obtain a three-dimensional model of the entire peptide. To identify structural details that justify the different behaviour of gH-combi compared to the parent peptide gH625, we started from the NMR structure of the latter (pdb code 2lqy) (Galdiero et al., 2012). The gH625 sequence, containing all L-residues, adopts a globally helical structure (Fig. 7, panel A). The gH-combi model was obtained from the 2lqy structure by inverting the chirality of the Leu^7, Trp^{10}, and Tyr^{13} residues without modifying the helical arrangement (Fig. 7, panel B). As can be seen from the comparison of the two

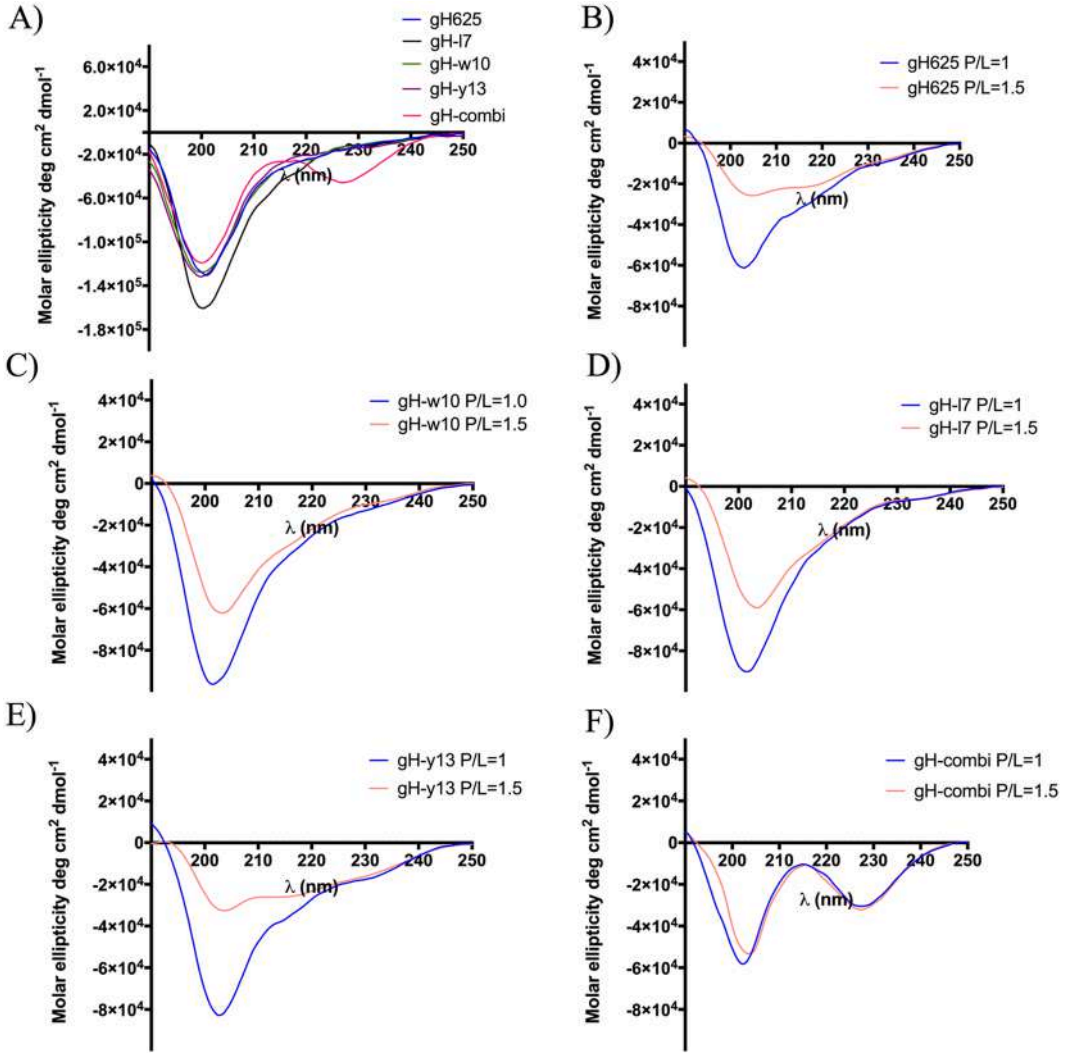

Fig. 4. CD spectra of gH625 and its derivatives in solution (A) and in liposomes at the peptide/lipid ratio of 0.5, 1, and 1.5 (B, C, D, E, F).

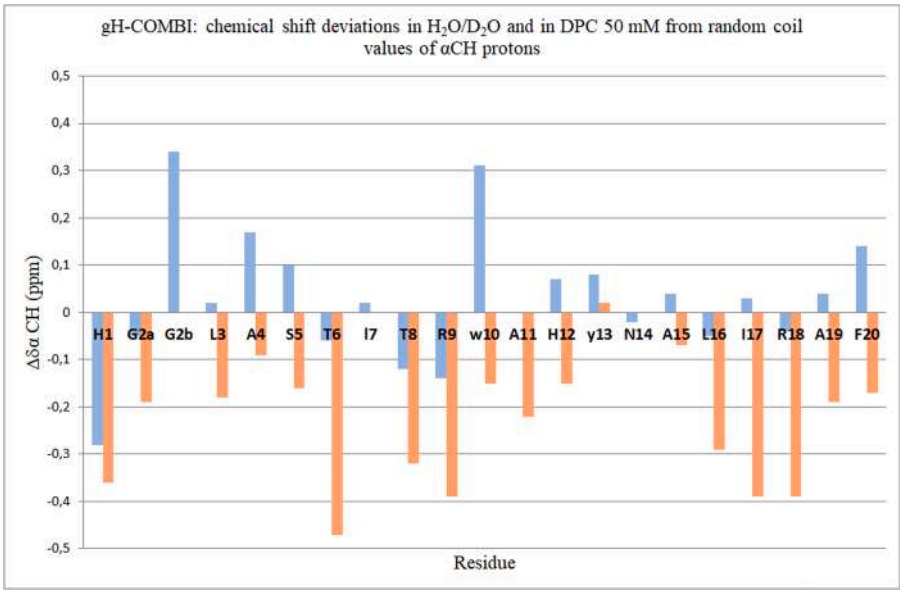

Fig. 5. Chemical shift deviations from random coil values of αCH protons of gH-combi in H_2O/D_2O 90/10 v/v (light blue bars) and in DPC 50 mM (orange bars). Residues at position 7, 10 and 13 are D-residues (D-Leu^7, D-Trp^{10}, and D-Tyr^{13}).

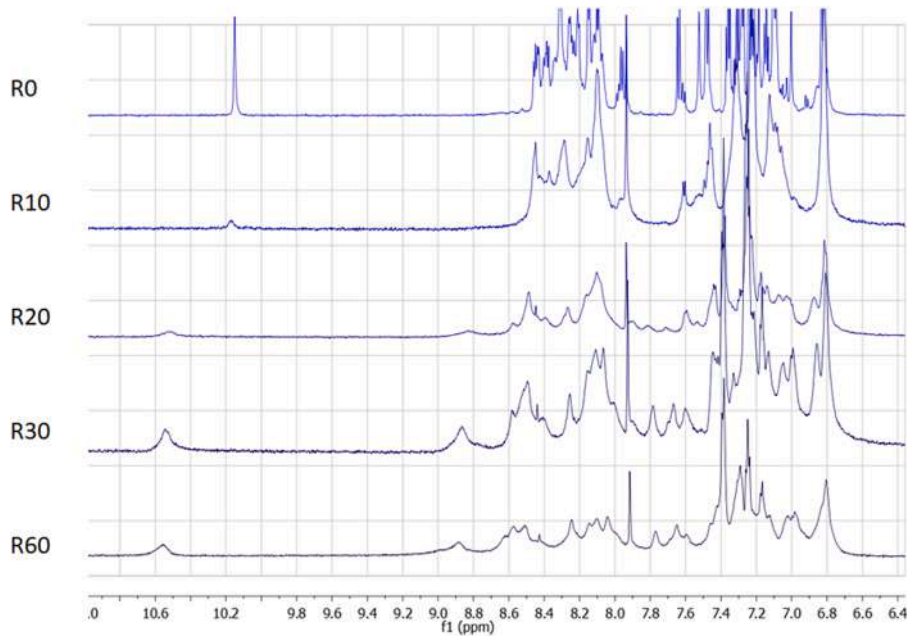

Fig. 6. Selection of 1D-NMR proton spectra (low-field region) of gH-combi acquired at increasing ratio R = DPC monomer /peptide. R60 corresponds to a DPC concentration of 20 mM and *ca.*2 micelle/peptide ratio.

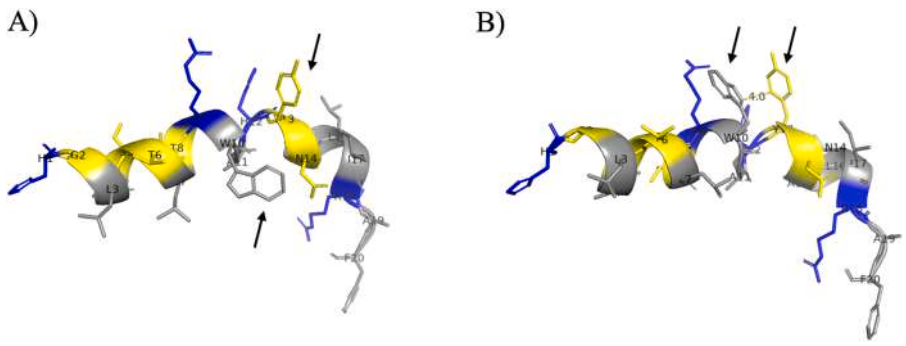

Fig. 7. Cartoon representation of A) first PDB structure of gH625 (PDB code 2lqy (Kalafatovic and Giralt, 2017)) and B) gH-combi model obtained from 2lqy by inverting the chirality of l7, w10 and y13 residues (indicated with the arrow). Side- chains are shown as sticks coloured by amino acid type: gray, hydrophobic; blue, basic; yellow, polar. Visual representation by using Pymol.

models in Fig. 7, the D-chirality of the two residues, w^{10} and y^{13}, in gH-combi isoorientate their aromatic side chains, making possible stacking interactions. This arrangement is not present in gH625. In addition, the interposition of His^{12} results in the formation of a cluster of isooriented aromatic side chains that along with stacking interactions between w^{10} and y^{13} may be responsible for the CD spectrum with the non-canonical minimum at 228 nm recorded in water and in the presence of SUVs. So, the region 10–13 may constitute a locus for peptide entry into the micelle/cell membrane.

3.6. Peptides induce lipid mixing

Previously, we demonstrated the peptide gH625 induced a significant membrane fusion resulting in a reduction in the fluorescence energy transfer efficiency between fluorophores 12-(N-methyl-N-(7-nitrobenz-2-oxa-1,3-diazol-4-yl) (NBD) and Rhodamine (Rho) bound to liposomes. To investigate the impact of the replacement of L-with D-isomers on the fusogenic activity, we used a population of LUVs (PC:Chol, 1:1) labelled with -NBD and -Rho used as acceptor and donor of fluorescence energy transfer, and then mixed with a population of unlabelled LUVs (PC:Chol, 1:1). The fusogenic activity of all peptides was calculated recording the dequenching of the donor fluorescence after the peptide addition at increasing concentrations. Here, we studied the ability of all peptides to induce complete fusion of vesicles at different peptide/lipide (P/L) ratios.

As observed in Fig. 8 (panel A), all peptides induced the membrane fusion with a different trend at a lipide/peptide ratio ranging from 0.02 to 0.1. When the three cleavage sites of gH625 were replaced by their D-isomers, we did not observe differences in fusogenic activity; in fact, gH625 and gH-combi showed similar membrane fusion determining the complete membrane fusion (100 %) at the highest P/L ratio of 0.1. Interestingly, when we just replaced W^{10} with D-form, the fusogenic activity increased significantly already at low P/L ratios, in fact, the peptide gH-w10 induced an effective lipid mixing (80 %) already at lowest P/L ratio of 0.01. Instead, the replacement of L^7 and Y^{13} caused a slight reduction in the fusogenic activity at low P/L ratio in comparison to gH625, but both induced complete lipid mixing (100 %) at the highest P/L ratio of 0.1.

In addition, we also investigated the ability of peptides to induce hemifusion of LUVs (PC:Chol) using the inner monolayer assay (Fig. 8, panel B). In this experiment, to measure the lipid mixing between the inner monolayers of vesicles in solution, the fluorescence from the LUVs' outer monolayer is eliminated by the addition of the reducing agent sodium dithionite. The peptides gH625 and gH-combi showed a low

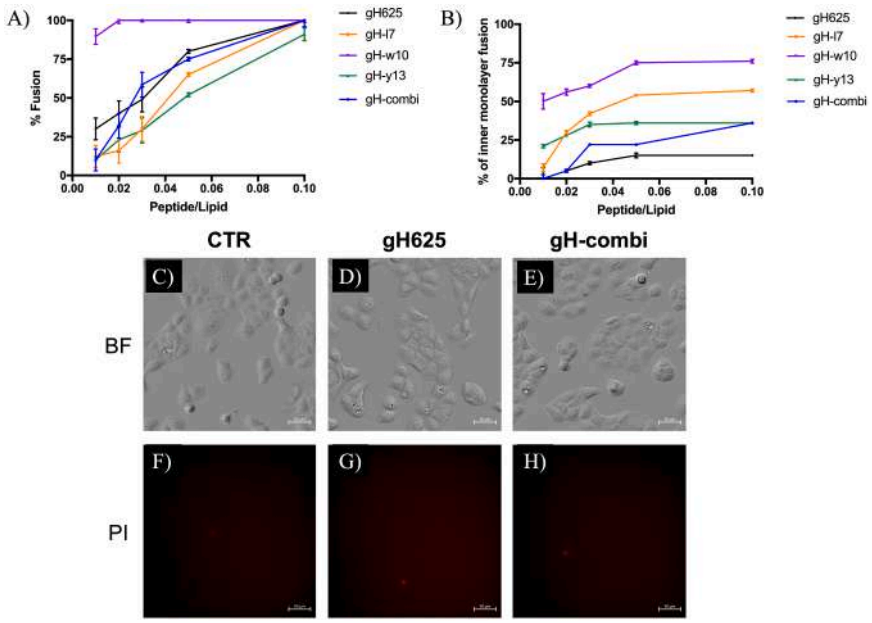

Fig. 8. Panel A reports the percentage of fusion ability of gH-625 and its derivatives using PC/Chol (1:1) LUVs. Panel B reports the percentage of inner monolayer fusion using PC/Chol (1:1) LUVs. Panels C–H: Membrane integrity assay of HaCaT cells following treatment with gH625 (D-G) or gH-combi (E-H) in comparison with the control (CTR, C and F). Representative microscopy images of HaCaT cells after 2 h of incubation with 5 μM of each peptide. Bright field: BF; Propidium iodide: PI. Bar size: 50 μM.

fusion of the inner monolayer reaching ~25 % of lipid mixing at the highest P/L of 0.1. Similarly to the fusion assay, the peptide gH-w10 showed high capacity to induce the inner monolayer fusion already at a low P/L ratio, determining ~50 % of inner monolayer fusion at the lowest P/L ratio of 0.01. Regarding the peptides gH-l7 and gH-y13, they both induced the inner monolayer fusion but with different trends compared with their behaviour in the fusion assay. Indeed, while the peptide gH-y13 induced a low inner monolayer fusion reaching ~35 % at the highest P/L ratio of 0.1, the peptide gH-l7 caused higher hemi-fusion ~55 % at the same P/L ratio.

In addition, to support further our hypothesis that peptides are able to diffuse inside lipidic vesicles as observed in lipid mixing assays and without involving pore formation, we performed the leakage assay using LUVs (PC:Chol) with encapsulated ANTS and DPX probes. In this experiment, if the peptides induce a bilayer perturbation through a pore formation, we should observe a release of ANTS and DPX from vesicles recording the increase of ANTS fluorescence. Interestingly, we did not observe liposome leakage (data not shown) because after the addition of each peptide ANTS was not released from LUVs even at highest P/L ratio of 0.5.

To further confirm the absence of pore formation, we performed a membrane integrity assay on HaCaT cells using propidium iodide (PI) staining. PI is a dye that cannot penetrate intact cell membranes and therefore serves as an indicator of membrane damage by fluorescing upon entry into compromised cells. For this assay, cells were treated with 5 μM of either gH-combi or the reference peptide gH625 for 2 h. As shown in Fig. 8 (panels C–H), the membranes of the cells treated with both peptides displayed normal, smooth membrane morphology and showed no evidence of PI uptake, similar to untreated control cell. These findings demonstrated that treatment with gH625 or gH-combi did not compromise cell membrane integrity, indicating an absence of pore formation.

3.7. Peptide insertion into lipid bilayer

The peptide insertion inside the membrane bilayer was measured exploiting the intrinsic fluorescence of the Trp residue located in the middle of the sequence. To evaluate the degree of Trp penetration in LUVs made of PC:Chol, we quenched it performing a titration with acrylamide at increasing concentrations from 0.02 M to 0.22 M. The acrylamide quencher is soluble in water and is not able to insert into the hydrophobic lipid bilayer; hence, more deeply a Trp is inserted, the less it is reached and quenched by acrylamide. The same experiment was also performed in water where the Trp is totally accessible to acrylamide.

As observed in Fig. 9, the Trp fluorescence of each peptide in water was completely quenched by acrylamide after addition of increasing concentrations from 0.02 M to 0.22 M, observing thus a reduction of the fluorescence emission of Trp at each concentration.

In contrast, the Trp is partially accessible to quenching by acrylamide in the presence of LUVs. After the incubation with LUVs, the quantum yield of Trp of all peptides is lower than that recorded in water due to the change in local environment upon interaction between peptide and lipid bilayer. Interestingly, for the peptides gH625 and gH-w10, in addition to reduction of the quantum yield, a blue shift of maximal spectral position toward shorter wavelength of 360 nm was also observed (Fig. 10, panels A and C), showing that both peptides are capable to penetrate in lipid bilayer.

To obtain a more quantitative evaluation of the peptide localization inside the lipid bilayer, Fig. 11 reports the titration adding acrylamide from 0.02 M to 0.22 M. The extent of Trp fluorescence decrease in the presence of the quencher, was much less evident than in water, revealing that the indole moiety is only partially accessible being instead inserted inside the LUVs (Fig. 11).

The accessibility of the indole to acrylamide in water and in LUVs was quantitatively evaluated by calculating Stern-Volmer constants (K_{sv}) obtained from linear regression of quenching data (Fig. 12). The value of K_{sv} is determined by the amount of not buried peptide as well as the fraction of the buried peptide inside the lipid bilayer. As reported in the Table 2, the values for K_{sv} in LUVs were lower than in solution for all peptides except for the derivative gH-w10. Indeed, while for all peptides the Trp was significantly inserted in the bilayer and completely

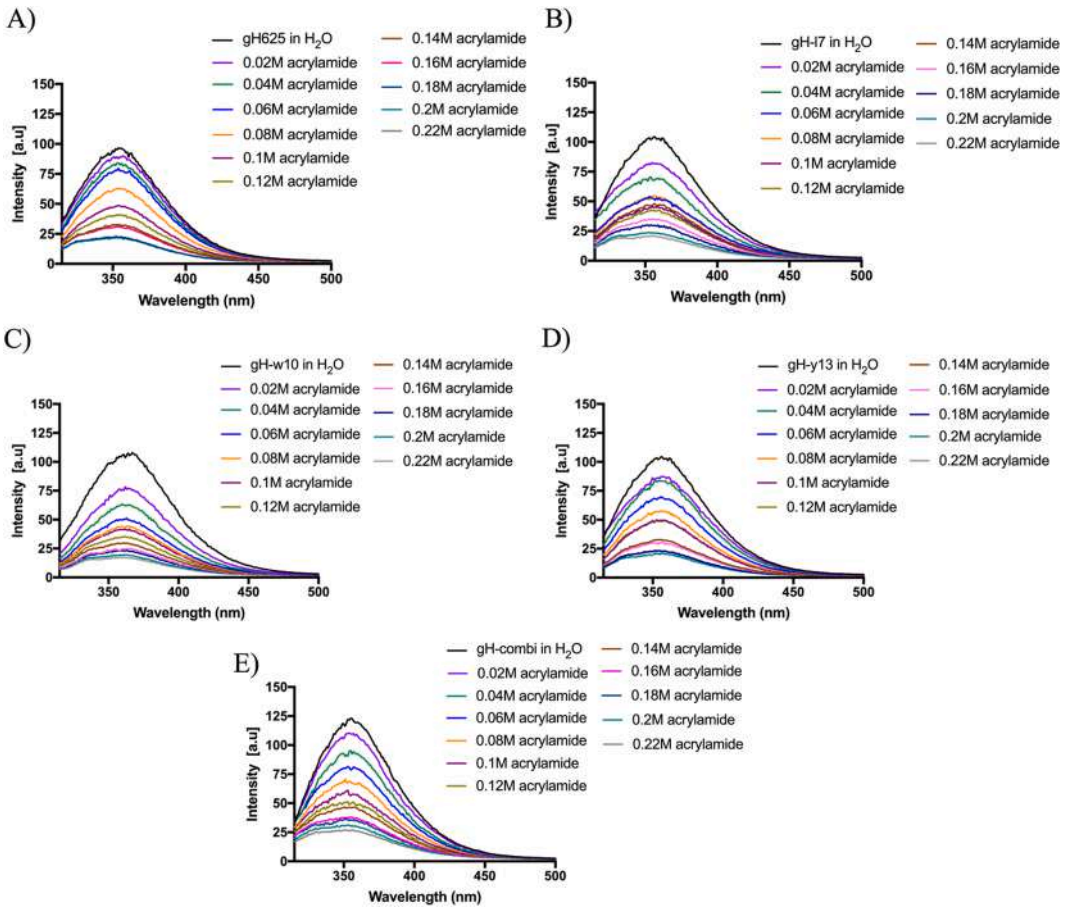

Fig. 9. Tryptophan fluorescence spectra for each peptide recorded in water at increasing concentrations of acrylamide from 0.02 M to 0.22 M.

accessible when in water, gH-w10 has similar K_{sv} (~10) values in both conditions, indicating that the peptide is only slightly inserted into the lipid bilayer and likely is already partially aggregated in aqueous solution.

In addition, the degree of penetration of peptides into LUVs was further investigated by recording the quenching of the Trp fluorescence by the bromo probes bound to the lipid chains of the membrane. We prepared LUVs containing two different phospholipids (25 % PC-Br in composition) with bromo quencher in: *i)* the positions 4,5 where the probe is located at the LUVs interface, *ii)* the positions 11,12 where the bromo is deeply buried into the lipid core. As observed in Fig. 13, the largest Trp quenching was measured in the presence of 11,12-Br LUVs for all peptides except for the peptide gH-w10. Indeed, the Trp fluorescence of the gH-w10 was significantly quenched in the presence of 4,5-Br LUVs because the Trp is not located into the lipid core as also demonstrated by the value of the constant Ksv. These results indicated that the indole moiety of gH625 and its derivatives gH-l7, gH-y13, and gH-combi is buried into the lipid bilayer, while the indole of gH-w10 is located at the interface between the lipid bilayer and the aqueous solution. In addition, these findings are in line with the intracellular ability of gH625 and its derivatives studied in living cells. In fact, gH-w10 displayed a reduced capacity to penetrate the cells likely because it establishes weaker interactions with phospholipids and lower insertion into lipid bilayer. On the contrary, the peptide gH-combi showed a strong interaction and insertion inside the lipid core that justified its significant ability to cross the cell membrane.

3.8. Proteolytic cut by chymotrypsin after membrane binding

To confirm the peptide insertion in the membrane, we performed the proteolytic cut by chymotrypsin after the incubation with small unilamellar vesicles (SUVs) made of PC:Chol. Chymotrypsin cleaves selectively peptide bonds formed by hydrophobic amino acids; if the Trp is buried in the lipid core, it is not exposed and accessible to the enzyme, hence its fluorescence does not change significantly. We recorded the changes in the quantum yield of Trp for each peptide before and after incubation with the enzyme both in buffer and in SUVs. As showed in Fig. 14, being the Trp completely exposed in buffer, it is easily recognized by the enzyme causing a large enhancement of the Trp fluorescence for all peptides except for gH-w10. In fact, we observed only a small increase of fluorescence after treatment with the enzyme; this is likely due to the fact that the Trp is partially buried also in aqueous solution by the formation of aggregates as also confirmed by the K_{sv} values.

In contrast, when the Trp is buried inside the lipid bilayer, it is not recognized and cut by the chymotrypsin, and we did not measure a significant increase of Trp fluorescence (Fig. 15). Firstly, each peptide was incubated with SUVs and the decrease of the Trp emission is caused by the peptide binding with liposomes, as already showed by our previous studies. When we added the enzyme to the peptide-lipid complex, we recorded a slight increase of Trp fluorescence, but it indicated that the peptide is protected against enzymatic digestion and the enzyme is not able to cleave its substrate. When prepared in LUVs also the Trp of gH-w10, although located towards the surface of the bilayer (as demonstrated by the Br experiments), is inaccessible to the enzyme. These results confirmed strong binding between peptide and

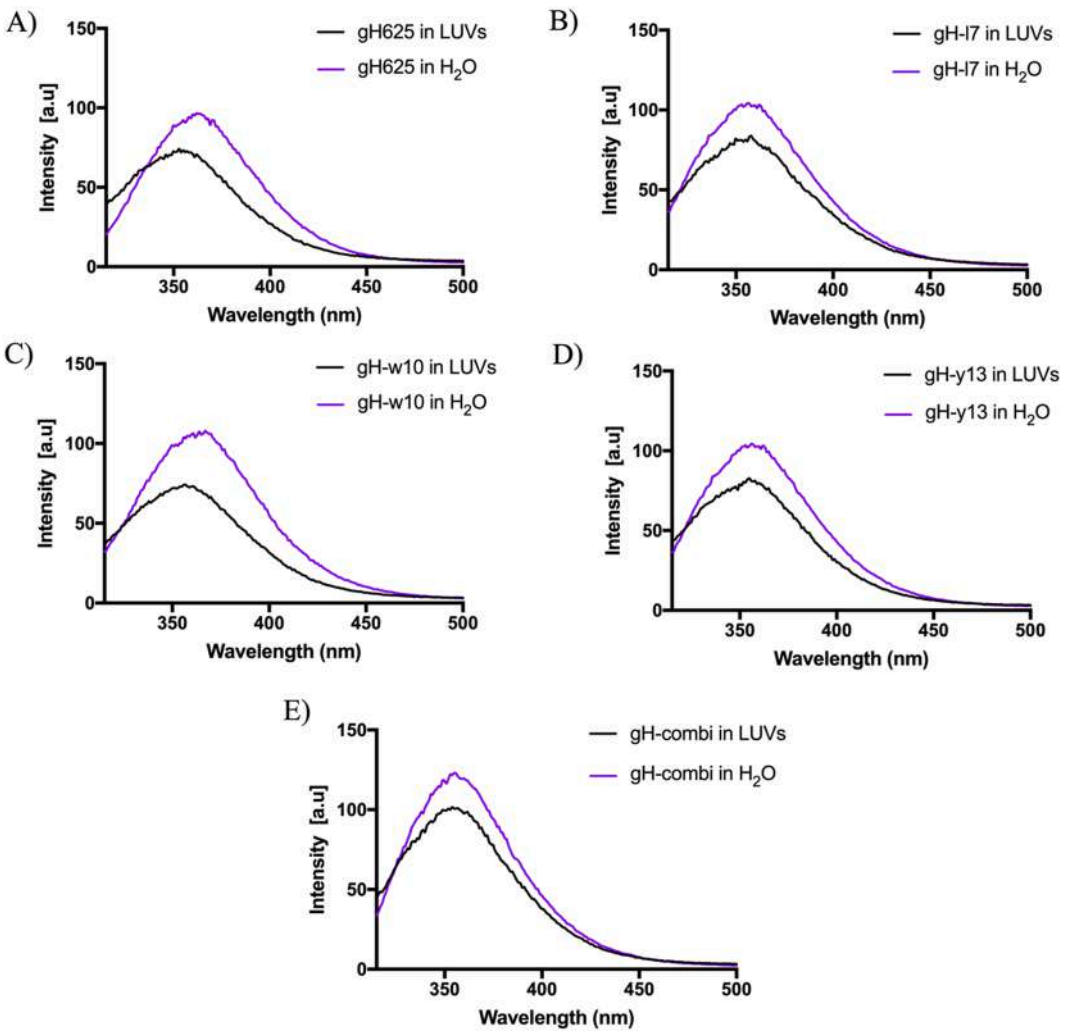

Fig. 10. Tryptophan fluorescence spectra for each peptide at the concentration of 10 μM recorded in water and after the incubation with LUVs made of PC:Chol.

phospholipid membranes and their insertion inside the lipid core or at the interface as observed in the previous experiments.

3.9. Cytotoxic activity of gH625 and its analogues on normal and cancer cells

The 3-(4,5-dimethyl-thiazol-2-yl)-2,5-diphenyltetrazolium bromide (MTT) assay was used to assess the cytotoxic activity of native peptide gH-625 and its four analogues in both normal HaCaT cells and A375 and RKO cancer cells. To this aim, cells were incubated with a wide range of peptide concentrations (from 1.25 to 40 μM) and tested for 24 h. The findings presented in Fig. 16 clearly show that none of the tested peptides significantly affected the viability of either cancerous or normal cells (Valiante et al., 2015). These results are consistent with our earlier research showing that gH-625 did not cause toxicity on SH-SY5Y and U-87 MG cancer cell lines (Valiante et al., 2015).

3.10. Safety profile of gH625 and gH-combi in the chicken embryo model

The chicken embryo model is a valuable method for assessing the safety profile of drug delivery systems, (Butler et al., 2022) providing an efficient alternative to traditional animal models in accordance with the 3R principles (Replacement, Reduction, and Refinement) (Buhr et al., 2020). To evaluate the potential toxicity of gH-625 and its most promising derivative, gH-combi, we performed an *in ovo* toxicity test (Fig. 17) (Adlia et al., 2018). The experimental solutions were injected *in ovo* into the albumen at the onset of embryogenesis, allowing for potential translocation throughout the entire organism (Sawosz et al., 2014). Specifically, fertilized eggs were divided into four groups on embryonic development day 3 (EDD3): the first and second groups received 5 μM of gH625 and gH-combi, respectively; the third group was injected with toluene as a positive control, and the fourth group received the vehicle as a negative control. The data presented in Fig. 17 indicate that the development of the chicken embryos was unaffected by either the native peptide or its derivative. Notably, all embryos injected with gH625 and gH-combi were viable and exhibited no significant developmental abnormalities at EDD8, EDD12, or EDD16, compared to control eggs, in accordance with the Hamburger and Hamilton stages (Hamburger and Hamilton, 1951). Furthermore, no differences were observed in the body weight or the weight of selected organs (liver and heart) in the chicken embryos on EDD16 after *in ovo* treatment with both peptides (Table 3). These findings strongly support the safety profile of the native peptide gH625 and its derivative gH-combi in an *in vivo* system.

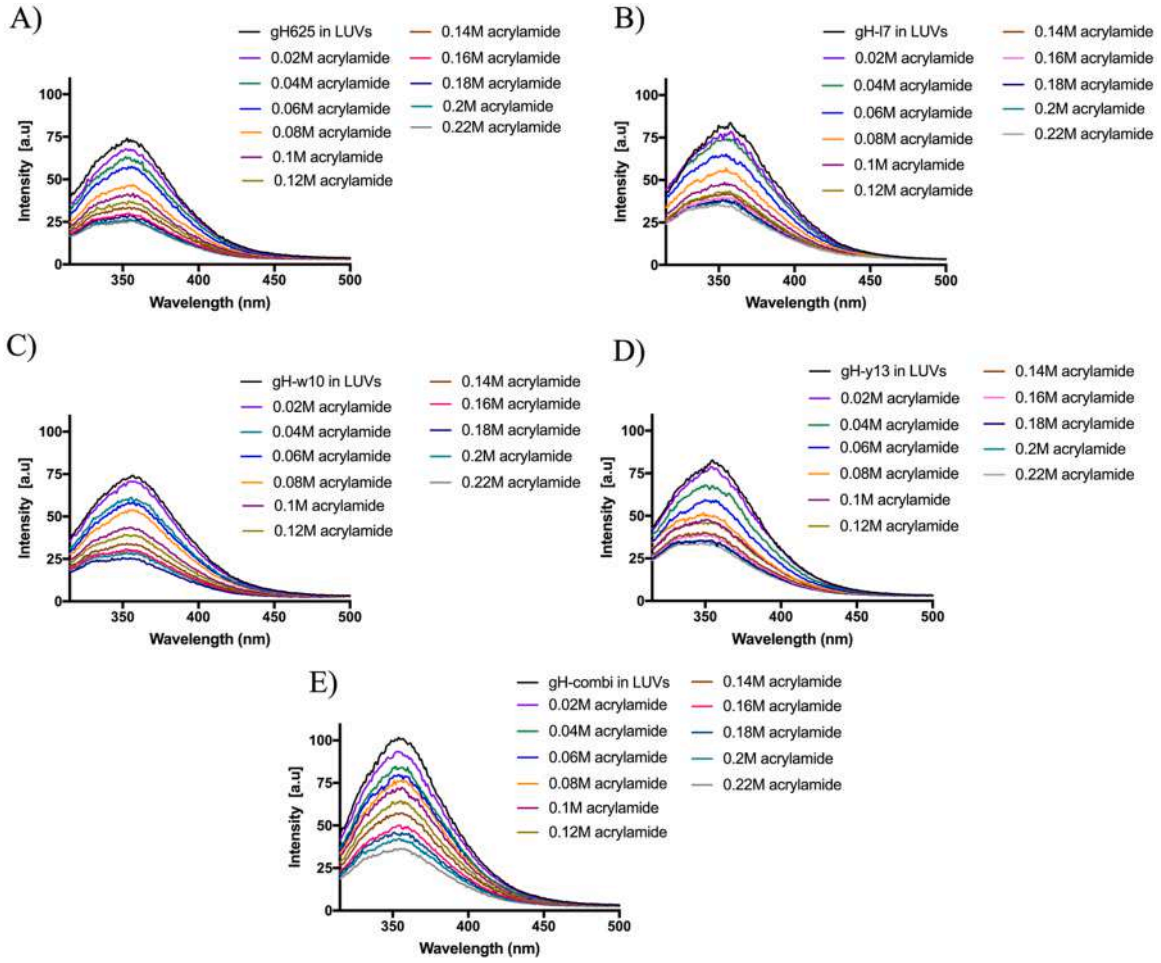

Fig. 11. Tryptophan fluorescence spectra for each peptide recorded in LUVs (PC:Chol) at increasing concentrations of acrylamide from 0.02 M to 0.22 M.

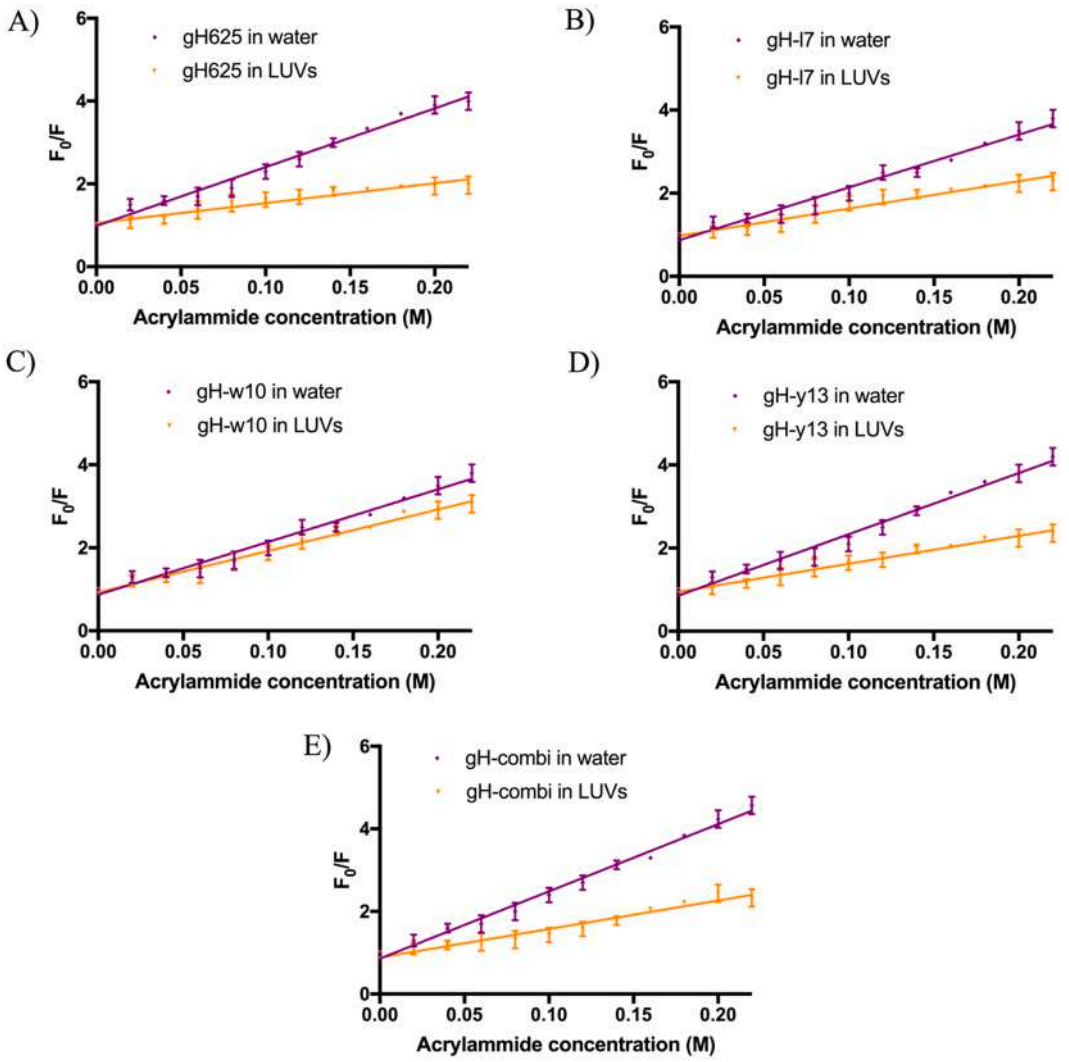

Fig. 12. Panels A–E report data analysed in buffer (purple line) and in LUVs (orange line) with the Stern-Volmer equation, $F_0/F = 1 + K_{sv}[Q]$, where F_0 and F represent the fluorescence intensities in the absence and the presence of the quencher (Q), respectively.

Table 2
Stern-Volmer (K_{sv}) quenching constants of peptides both in water and LUVs.

Peptide	K_{sv} constant value (in water)
gH625	14.2 ± 0.6
gH-l7	12.7 ± 0.6
gH-w10	11.5 ± 0.7
gH-y13	14.8 ± 0.6
gH-combi	16.4 ± 0.6
Peptide	**K_{sv} constant value (in LUVs)**
gH625	4.8 ± 0.3
gH-l7	6.6 ± 0.4
gH-w10	10.0 ± 0.4
gH-y13	6.7 ± 0.3
gH-combi	6.9 ± 0.5

4. Discussions

The peptide gH625 can interact with and cross cell membranes without causing leakage or pore formation, relying on temporary and local membrane destabilization. However, its susceptibility to proteases like chymotrypsin reduces its intracellular half-life. To address this, we replaced amino acids involved in the peptide's degradation (L7, W10, and Y13) with their D-enantiomers, which are less prone to enzymatic cleavage. Here, we reported a series of experiments aimed at demonstrating the stability and functionality of gH625 analogues without compromising the cell-penetrating ability. Furthermore, we provide the results of studies characterizing the biosafety profiles of these gH625 analogues, both *in vitro* and *in vivo*.

The stability of the analogues in the presence of chymotrypsin was measured over time. Interestingly, the peptides with only one D-enantiomeric substitution (gH-l7, gH-w10, gH-y13) showed similar degradation patterns to gH-625, indicating that all the positions were equally prone to degradation. However, the gH-combi analogue demonstrated improved resistance to degradation, with ~50 % of the intact peptide remaining after 120 min of incubation, compared to 15 min for the others. Interestingly, in the internalization assay, the gH-combi peptide showed the highest internalization efficiency (nearly 90 %), while gH-y13 exhibited a similar internalization rate to the native peptide gH-625. gH-l7 and gH-w10 showed lower internalization rates, with gH-w10 being the least efficient. At this point we wanted to analyse the effect of the D-enantiomers on the secondary structure and mechanism of interactions with model membranes to better unravel the differences in cellular uptake.

The structural conformation of the peptides was studied in water and in membrane-mimicking environments (SUVs). In water, most peptides adopted a random coil structure, except for gH-combi, which showed also a non-canonical peak at 228 nm although being mainly random as

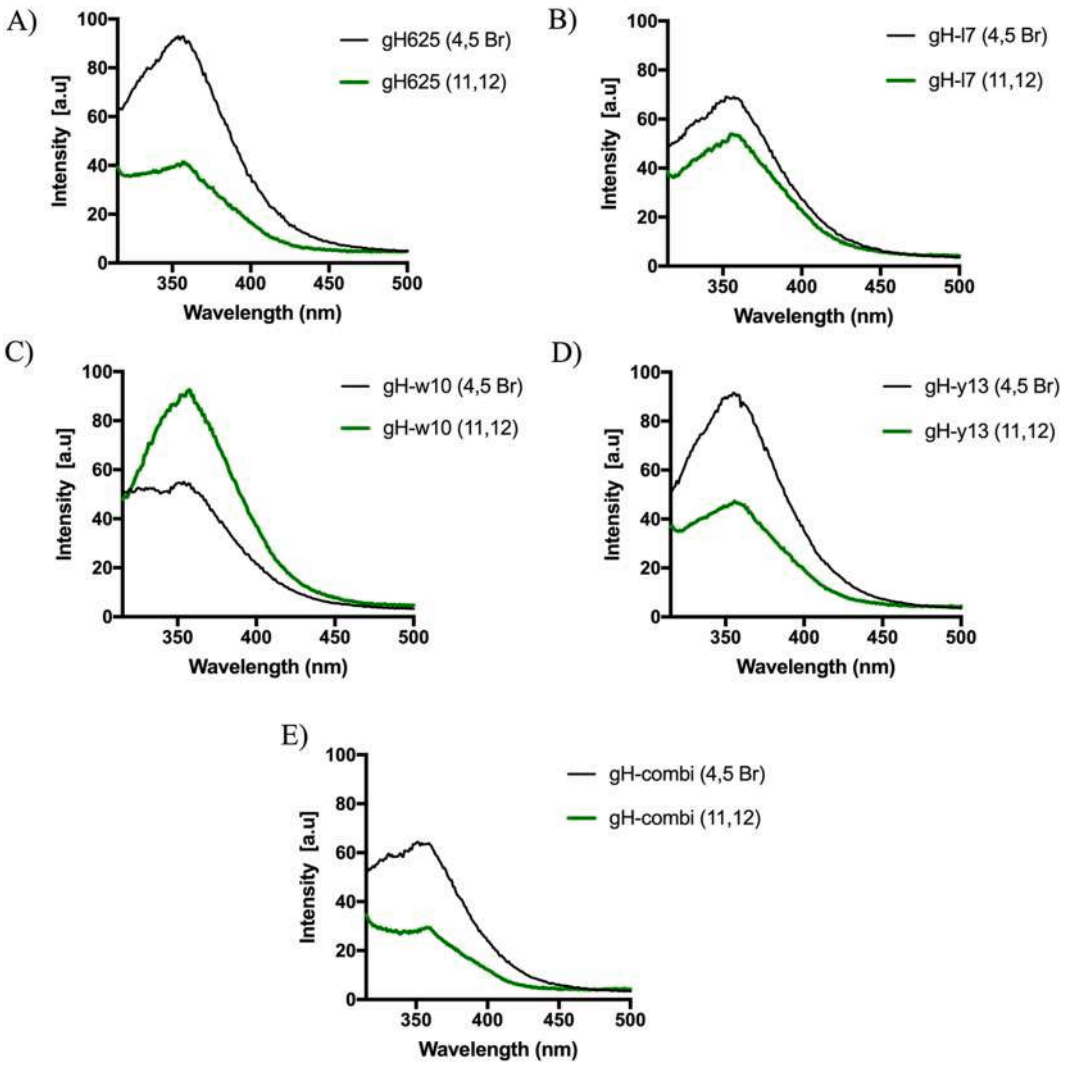

Fig. 13. Tryptophan fluorescence spectra for each peptide recorded in LUVs (PC:Chol) bearing the probes 4,5-Br-PC and 11,12-Br-PC.

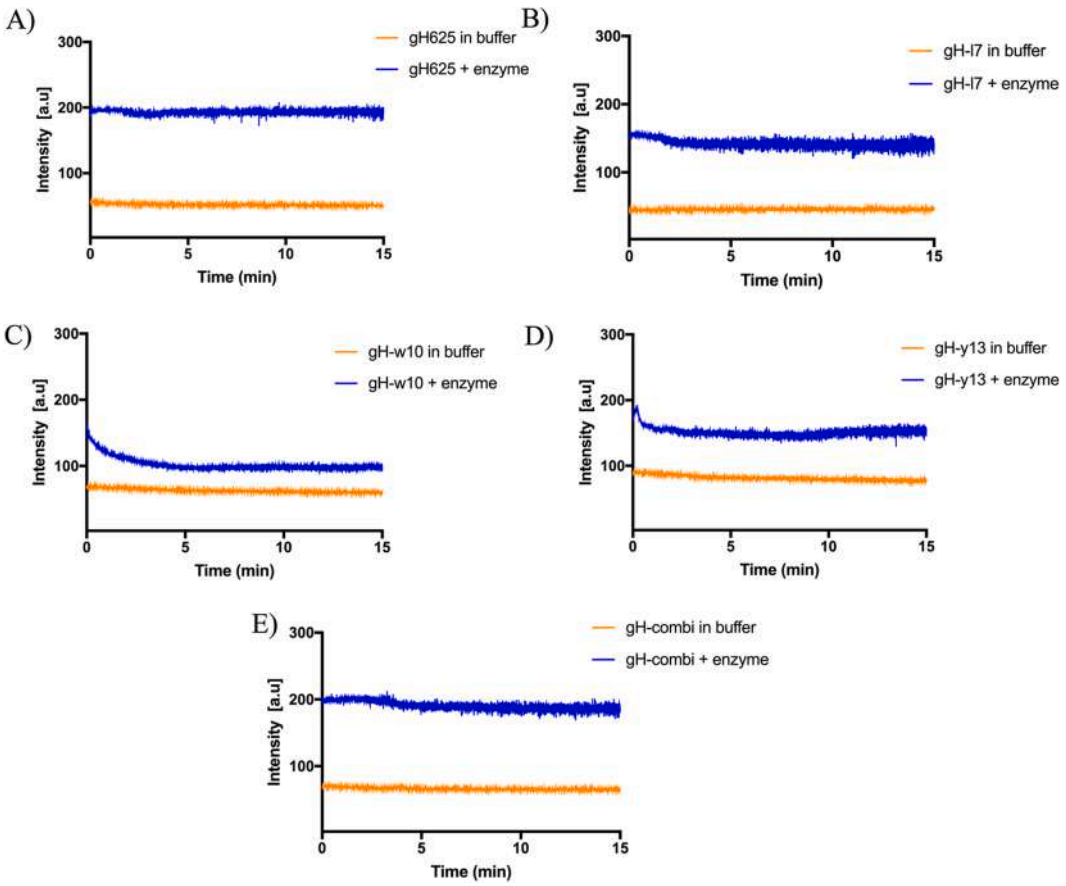

Fig. 14. The fluorescence emission of each peptide with excitation set at 355 nm in buffer before and after the proteolytic cut by chymotrypsin.

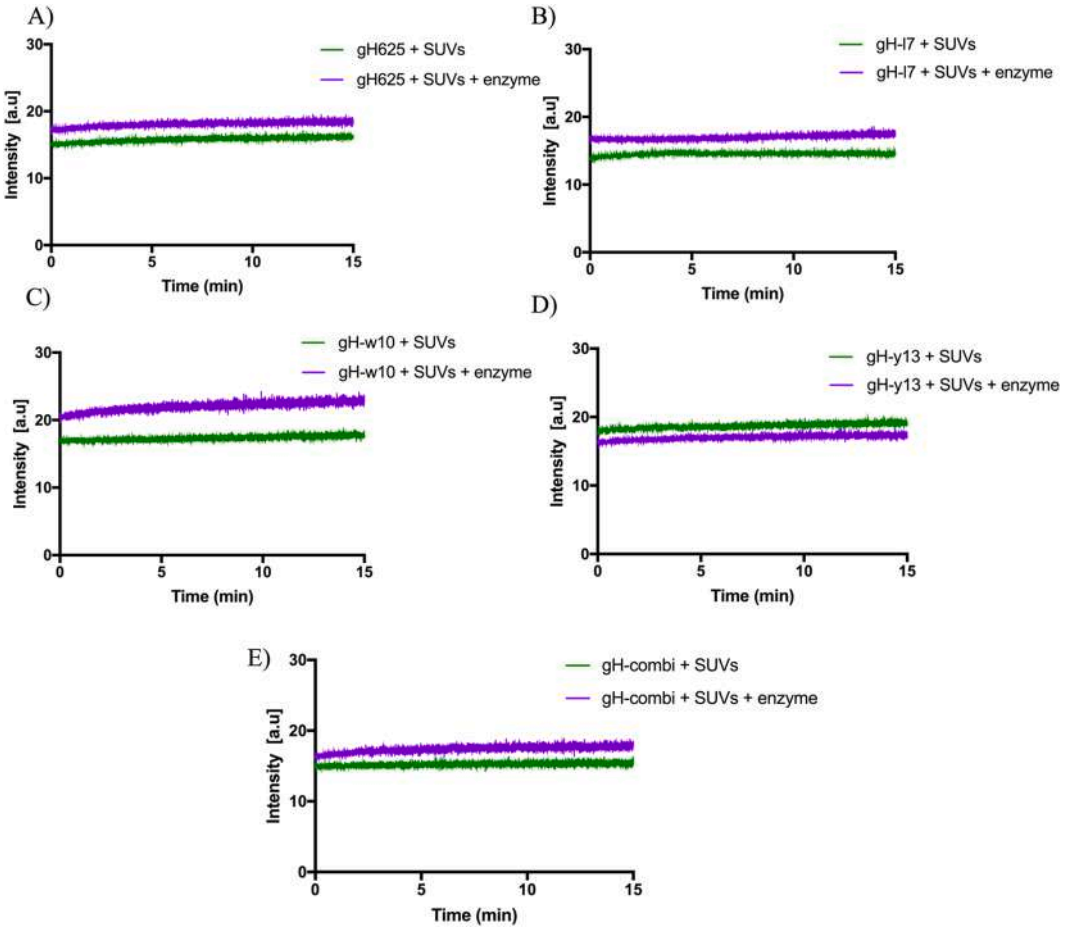

Fig. 15. The fluorescence emission of each peptide with excitation set at 355 nm in SUVs before and after the proteolytic cut by chymotrypsin.

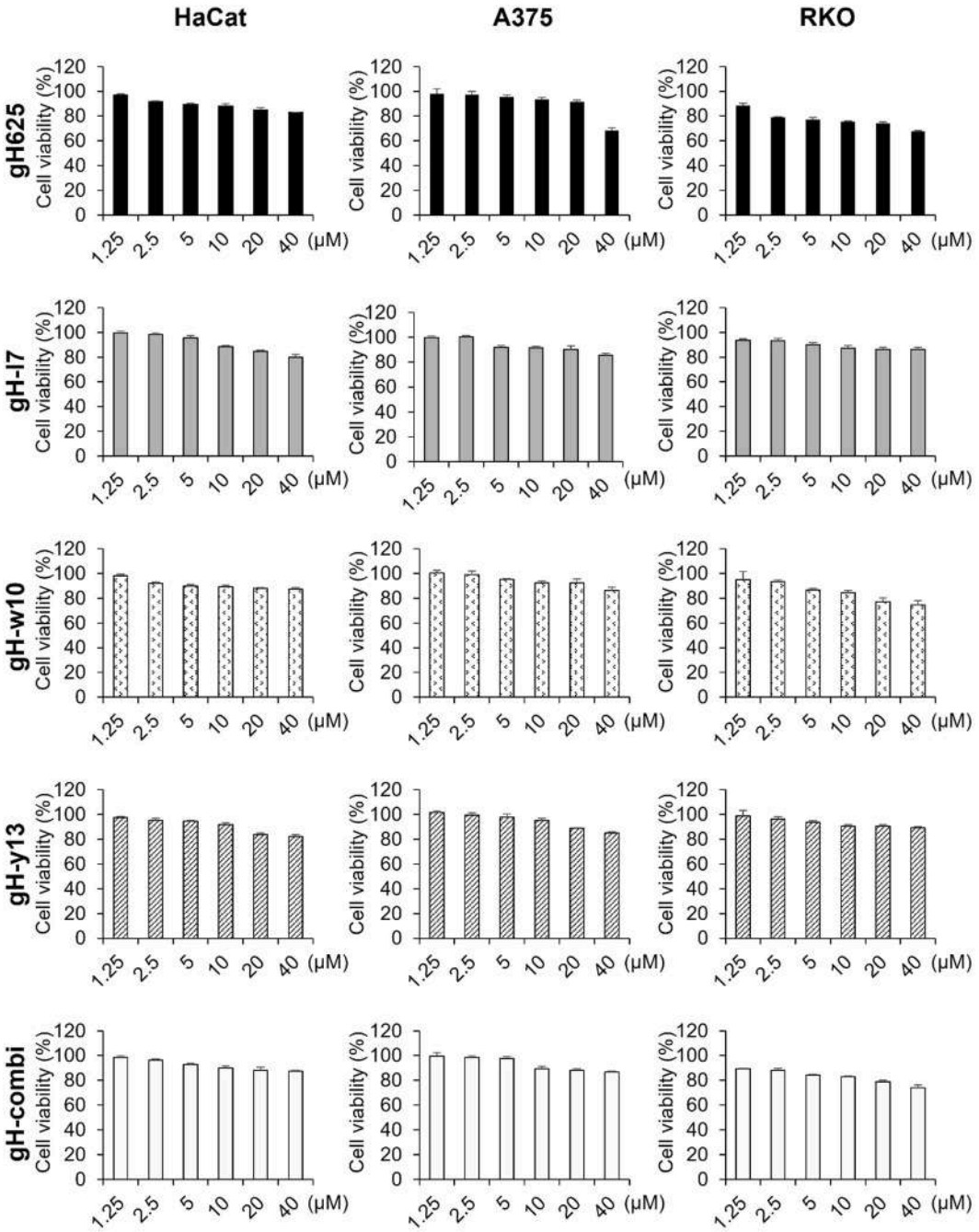

Fig. 16. Cytotoxic activity of gH625 and its derivatives. HaCat, A375 and RKO cells were treated with a wide range of peptides (from 1.25 to 40 μM). After 24 h, cell viability was assessed by the MTT assay. Bars represent the mean of triplicate experiments; error bars represent the standard deviation.

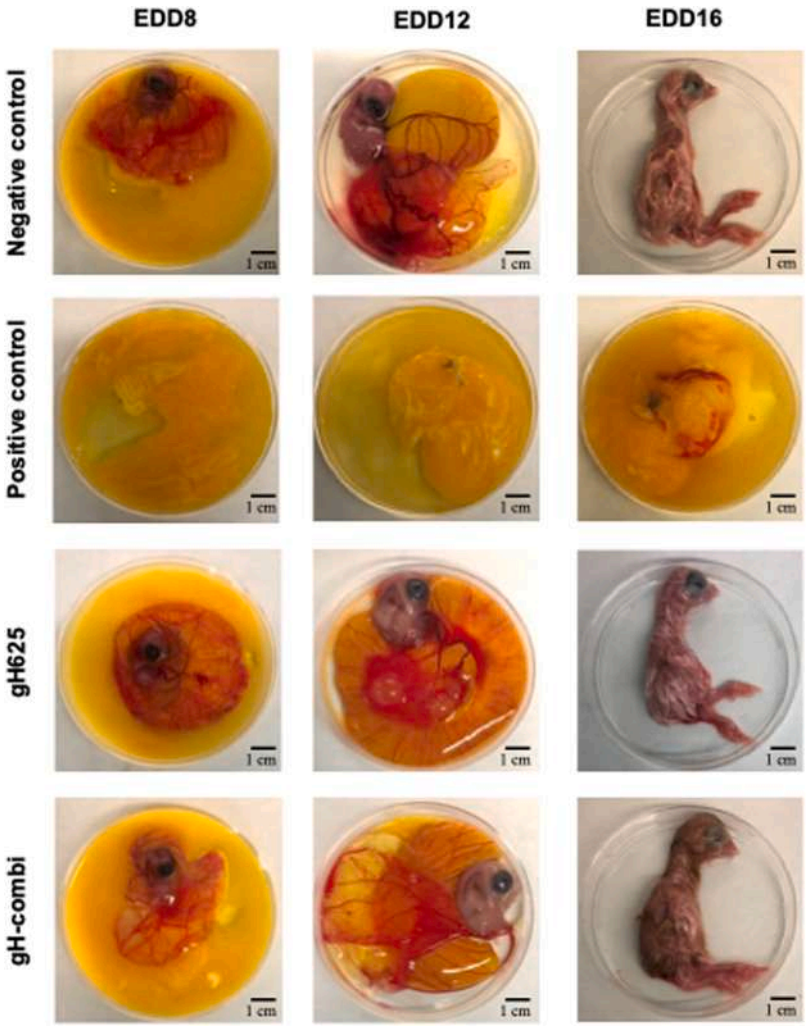

Fig. 17. In ovo toxicity test of gH625 and its analogue gH-combi. Fertilized chicken eggs were incubated in a rotating incubator at 37.8 °C and 50 % relative humidity. The first day of incubation was designated as embryonic development day (EDD) zero (EDD0). On EDD3, eggs were injected with 5 μM of gH625 or gH-combi. Toluene injection was used as a positive control, and the vehicle was injected into the negative control group. Images of the chicken embryos were captured on EDD8, EDD12, and EDD16.

Table 3
Weight of the embryo body and selected organs, evaluated according to the Hamburger-Hamilton development stages (HH), and mortality of chicken embryos at EDD16 after in ovo injection with gH625 and gH-combi[a].

Indices	Groups			ANOVA	
	Control	gH625	gH-combi	SEM	*p*-value
Body weight *	15.9	13.5	16.5	0.856	ns
Liver	0.642	0.547	0.503	0.041	ns
Heart	0.119	0.127	0.103	0.007	ns
HH	correct	correct	correct	–	–
Mortality %	6	0	6	–	–

* Embryos weighed without the yolk sac; ns = non-significant, $p < 0.05$.
[a] Organ weights (absolute weights) and body weights are given in grams.

also confirmed by NMR. In the presence of SUVs, gH-625 and gH-y13 adopted helical conformations, whereas gH-w10 and gH-l7 maintained random coil structures. Interestingly, the CD spectrum in SUVs of gH-combi shows again a minimum at 228 nm. Furthermore, in micellar environments, NMR showed that gH-combi adopts mainly helical conformations; we believe that this conformational change is crucial for the membrane interaction and insertion as for its parent peptide gH-625. Specifically, NMR data, as chemical shift variations and line broadening upon increasing DPC additions, testify the ability of gH-combi to interact with micelles. While chemical shift deviations indicate the stabilization of a helical structure, the line broadening produces a NOE pattern that is not suitable for obtaining three-dimensional structures. The gH-combi model obtained from the 2lqy structure by inverting the chirality of the residues of Leu7, Trp10 and Tyr13 shows that, unlike the native peptide gH-625, it has a cluster of isooriented aromatic side chains, formed by w10, His12 and y13. The NMR data together with the CD spectra likely support the hypothesis of the formation of a π stacking interaction which produces the non-canonical band at the CD and represents a good site for peptide penetration into the cell micelle/membrane. This structural feature may account for the better penetration properties of gH-combi compared to gH-625 that lacks the aromatic cluster.

The mechanism of action of all derivatives was explored using different biophysical techniques. The fusogenic activity of the peptides was assessed using LUVs made of PC:Chol (1:1) to mimic eukaryotic membranes. All peptides induced lipid mixing, but gH-w10 was particularly effective at lower peptide concentrations, while gH-combi exhibited similar activity to gH-625. The peptides did not induce significant hemifusion, except for gH-w10, which showed higher activity in the inner monolayer fusion assay. This is in line also with the results of the fluorescence quenching assays, evaluating the insertion of peptides

into lipid bilayers. gH-625 and gH-combi inserted deeply into the lipid bilayer, as indicated by reduced accessibility to acrylamide, whereas gH-w10 showed less insertion. Interestingly, gH-w10 also showed a low accessibility of the Trp in aqueous solution, indicating that it is likely already partially aggregated in water. When we performed the accessibility of Trp to chymotrypsin in water and in LUVs these results were confirmed, indicating that the Trp is available to the enzyme in water for all the analogues except gH-w10; while it is not accessible when the analogues are inserted in LUVs.

The biosafety profile of gH-625 analogues was assessed by testing the cytotoxicity of the peptides in both normal HaCaT cells and cancer cell lines (A375, RKO). The results, which showed no significant toxic effects at any of the concentrations tested, suggest that the peptides may have a favorable safety profile in terms of cell viability. To further validate these findings, we used the chicken embryo model, which has become a valuable preclinical system bridging the gap between *in vitro* and *in vivo* mammalian models (Sarnella et al., 2024). For this experiment, we selected gH-625 and its most promising derivative, gH-combi. Our results demonstrated that both peptides were non-toxic, as evidenced by the high survival rate of the embryos. The *in ovo* administration of both peptides did not affect embryo development or the weight of the body, heart, and liver. These findings strongly support the safety profiles of gH-625 and gH-combi, not only in cellular models but also in a living organism.

5. Conclusions

This comprehensive study demonstrates the design of analogues with enhanced stability and cell-penetrating capability, without compromising safety. The findings highlight the potential of gH625 and of gH-combi for intracellular delivery applications, particularly in drug delivery or gene therapy. The D-amino acids modification strategy successfully improved gH-625 resistance to proteases, while preserving its membrane-crossing ability, making gH-combi the most promising candidate.

CRediT authorship contribution statement

Rosa Bellavita: Writing – original draft, Methodology, Investigation, Data curation, Conceptualization. **Annalisa Pecoraro:** Writing – original draft, Methodology, Data curation. **Sara Palladino:** Methodology, Data curation. **Camilla Danisi:** Methodology, Data curation. **Annarita Falanga:** Methodology, Investigation, Conceptualization. **Gabriella D'Auria:** Writing – original draft, Conceptualization. **Lucia Falcigno:** Writing – original draft, Conceptualization. **Giulia Russo:** Writing – original draft, Visualization, Methodology, Investigation, Funding acquisition, Conceptualization. **Stefania Galdiero:** Writing – original draft, Visualization, Methodology, Investigation, Funding acquisition, Conceptualization. **Annapina Russo:** Writing – original draft, Visualization, Methodology, Investigation, Funding acquisition, Conceptualization.

Declaration of competing interest

The authors declare that they have no conflicts of interest

Acknowledgments

This research was funded by the grant PRIN2022-MUR (Code:2022JXSA9C and CUP E53D23012520006). This research was supported by the grant "National Center for Gene Therapy and Drugs based on RNA Technology" financed by the European Union - Next Generation EU, Project CN00000041, CUP UNINA: E63C22000940007, Spoke 8 "Platforms for RNA/DNA delivery".

Supplementary materials

Supplementary material associated with this article can be found, in the online version, at doi:10.1016/j.ejps.2025.107204.

Data availability

Data will be made available on request.

References

Adlia, A., Tomagola, I., Damayanti, S., Mulya, A., Rachmawati, H., 2018. Antifibrotic activity and In ovo toxicity study of liver-targeted curcumin-gold nanoparticle. Sci. Pharm. 86, E41.
Aguilera, J., Vazquez-Reyes, S., Sun, J., 2021. A fluorescence dequenching-based liposome leakage assay to measure membrane permeabilization by pore-forming proteins. Bio. Protoc. 11, e4025.
Al Musaimi, O., Lombardi, L., Williams, D.R., Albericio, F., 2022. Strategies for improving peptide stability and delivery. Pharmaceuticals (Basel) 15, 1283.
Barra, T., Falanga, A., Bellavita, R., Laforgia, V., Prisco, M., Galdiero, S., Valiante, S., 2022. gH625-liposomes deliver PACAP through a dynamic *in vitro* model of the blood-brain barrier. Front. Physiol. 13, 932099.
Bellavita, R., Braccia, S., Galdiero, S., Falanga, A., 2023a. Glycosylation and lipidation strategies: approaches for improving antimicrobial peptide efficacy. Pharmaceuticals (Basel) 16, 439.
Bellavita, R., Maione, A., Braccia, S., Sinoca, M., Galdiero, S., Galdiero, E., Falanga, A., 2023b. Myxinidin-derived peptide against biofilms caused by cystic fibrosis emerging pathogens. Int. J. Mol. Sci. 24, 3092.
Bellavita, R., Falanga, A., Merlino, F., D'Auria, G., Molfetta, N., Saviano, A., Maione, F., Galdiero, U., Catania, M.R., Galdiero, S., Grieco, P., Roscetto, E., Falcigno, L., Buommino, E., 2023c. Unveiling the mechanism of action of acylated temporin L analogues against multidrug-resistant Candida albicans. J. Enzyme Inhib. Med. Chem. 38, 36–50.
Bellavita, R., Piccolo, M., Leone, L., Ferraro, M.G., Dardano, P., De Stefano, L., Nastri, F., Irace, C., Falanga, A., Galdiero, S., 2024. Tuning peptide-based nanofibers for achieving selective doxorubicin delivery in triple-negative breast cancer. Int. J. Nanomedicine. 19, 6057–6084.
Bolen, E.J., Holloway, P.W., 1990. Quenching of tryptophan fluorescence by brominated phospholipid. Biochemistry 29, 9638–9643.
Bottens, R.A., Yamada, T., 2022. Cell-penetrating peptides (CPPs) as therapeutic and diagnostic agents for cancer. Cancers (Basel) 14, 5546.
Brignola, C., Pecoraro, A., Danisi, C., Iaccarino, N., Di Porzio, A., Romano, F., Carotenuto, P., Russo, G., Russo, A., 2024. uL3 Regulates redox metabolism and ferroptosis sensitivity of p53-deleted colorectal cancer cells. Antioxidants (Basel) 13, 757.
Brooks, H., Lebleu, B., Vives, E., 2005. Tat peptide-mediated cellular delivery: back to basics. Adv. Drug. Deliv. Rev. 57, 559–577.
Buhr, C.R., Wiesmann, N., Tanner, R.C., Brieger, J., Eckrich, J., 2020. The chorioallantoic membrane assay in nanotoxicological research-an alternative for. *In Vivo* Experimentation. Nanomaterials (Basel) 10, 2328.
Butler, K.S., Brinker, C.J., Leong, H.S., 2022. Bridging the *In vitro* to *In vivo* gap: using the chick embryo model to accelerate nanoparticle validation and qualification for *In vivo* studies. ACS Nano 16, 19626–19650.
Cho, I., Jackson, M.R., Swift, J., 2016. Roles of cross-membrane transport and signaling in the maintenance of cellular homeostasis. Cell. Mol. Bioeng. 9, 234–246.
Cleal, K., He, L., Watson, P.D., Jones, A.T., 2013. Endocytosis, intracellular traffic and fate of cell penetrating peptide based conjugates and nanoparticles. Curr. Pharm. Des. 19, 2878–2894.
Conte, C., Longobardi, G., Barbieri, A., Palma, G., Luciano, A., Dal Poggetto, G., Avitabile, C., Pecoraro, A., Russo, A., Russo, G., Laurienzo, P., Romanelli, A., Quaglia, F., 2023. Non-covalent strategies to functionalize polymeric nanoparticles with NGR peptides for targeting breast cancer. Int. J. Pharm. 633, 122618.
Cummings, J.E., Vanderlick, T.K., 2007. Aggregation and hemi-fusion of anionic vesicles induced by the antimicrobial peptide cryptdin-4. Biochim. Biophys. Acta. 1768, 1796–1804.
De Filippis, D., Russo, A., De Stefano, D., Cipriano, M., Esposito, D., Grassia, G., Carnuccio, R., Russo, G., Iuvone, T., 2014. Palmitoylethanolamide inhibits rMCP-5 expression by regulating MITF activation in rat chronic granulomatous inflammation. Eur. J. Pharmacol. 725, 64–69.
Del Genio, V., Bellavita, R., Falanga, A., Herve-Aubert, K., Chourpa, I., Galdiero, S., 2022. Peptides to overcome the limitations of current anticancer and antimicrobial nanotherapies. Pharmaceutics 14, 1235.
Dinca, A., Chien, W.M., Chin, M.T., 2016. Intracellular delivery of proteins with cell-penetrating peptides for therapeutic uses in Human disease. Int. J. Mol. Sci. 17, 263.
Dowaidar, M., 2024. Uptake pathways of cell-penetrating peptides in the context of drug delivery, gene therapy, and vaccine development. Cell. Signal. 117, 111116.
Falanga, A., Vitiello, M.T., Cantisani, M., Tarallo, R., Guarnieri, D., Mignogna, E., Netti, P., Pedone, C., Galdiero, M., Galdiero, S., 2011. A peptide derived from herpes simplex virus type 1 glycoprotein H: membrane translocation and applications to the delivery of quantum dots. Nanomedicine 7, 925–934.
Feng, Z., Xu, B., 2016. Inspiration from the mirror: D-amino acid containing peptides in biomedical approaches. Biomol. Concepts. 7, 179–187.

Frallicciardi, J., Gabba, M., Poolman, B., 2022. Determining small-molecule permeation through lipid membranes. Nat. Protoc. 17, 2620–2646.
Fukuta, T., Kogure, K., 2022. Biomimetic nanoparticle drug delivery systems to overcome biological barriers for therapeutic applications. Chem. Pharm. Bull (Tokyo). 70, 334–340.
Galdiero, S., Falanga, A., Vitiello, M., Raiola, L., Fattorusso, R., Browne, H., Pedone, C., Isernia, C., Galdiero, M., 2008. Analysis of a membrane interacting region of herpes simplex virus type 1 glycoprotein H. J. Biol. Chem. 283, 29993–30009.
Galdiero, S., Falanga, A., Vitiello, M., Raiola, L., Russo, L., Pedone, C., Isernia, C., Galdiero, M., 2010. The presence of a single N-terminal histidine residue enhances the fusogenic properties of a membranotropic peptide derived from herpes simplex virus type 1 glycoprotein H. J. Biol. Chem. 285, 17123–17136.
Galdiero, S., Russo, L., Falanga, A., Cantisani, M., Vitiello, M., Fattorusso, R., Malgieri, G., Galdiero, M., Isernia, C., 2012. Structure and orientation of the gH625-644 membrane interacting region of herpes simplex virus type 1 in a membrane mimetic system. Biochemistry 51, 3121–3128.
Gesualdo, C., Balta, C., Platania, C.B.M., Trotta, M.C., Herman, H., Gharbia, S., Rosu, M., Petrillo, F., Giunta, S., Della Corte, A., Grieco, P., Bellavita, R., Simonelli, F., D'Amico, M., Hermenean, A., Rossi, S., Bucolo, C., 2021. Fingolimod and diabetic retinopathy: a drug repurposing study. Front. Pharmacol. 12, 718902.
Ghorai, S.M., Deep, A., Magoo, D., Gupta, C., Gupta, N., 2023. Cell-penetrating and targeted peptides delivery systems as potential pharmaceutical carriers for enhanced delivery across the blood-brain barrier (BBB). Pharmaceutics 15, 1999.
Gori, A., Lodigiani, G., Colombarolli, S.G., Bergamaschi, G., Vitali, A., 2023. Cell penetrating peptides: classification, mechanisms, methods of study, and applications. ChemMedChem. 18, e202300236.
Hamburger, V., Hamilton, H.L., 1951. A series of normal stages in the development of the chick embryo. J. Morphol. 88, 49–92.
Hazrati, M.K., Vacha, R., 2024. Membrane adsorption enhances translocation of antimicrobial peptide buforin 2. J. Phys. Chem. B. 128, 8469–8476.
Jafari, S., Maleki Dizaj, S., Adibkia, K., 2015. Cell-penetrating peptides and their analogues as novel nanocarriers for drug delivery. Bioimpacts 5, 103–111.
Jiao, C.Y., Delaroche, D., Burlina, F., Alves, I.D., Chassaing, G., Sagan, S., 2009. Translocation and endocytosis for cell-penetrating peptide internalization. J. Biol. Chem. 284, 33957–33965.
Kalafatovic, D., Giralt, E., 2017. Cell-penetrating peptides: design strategies beyond primary structure and amphipathicity. Molecules 22, 1929.
Kim, S.M., Faix, P.H., Schnitzer, J.E., 2017. Overcoming key biological barriers to cancer drug delivery and efficacy. J. Control. Release. 267, 15–30.
Klug, J., Berberian, M.V., Lopez Marti, J.M., Mayorga, L.S., Del Popolo, M.G., 2024. Membrane binding strength *vs* pore formation cost horizontal line what drives the Membrane permeation of nanoparticles coated with cell-penetrating peptides? J. Phys. Chem. B. 128, 937–948.
Kou, L., Bhutia, Y.D., Yao, Q., He, Z., Sun, J., Ganapathy, V., 2018. Transporter-guided delivery of nanoparticles to improve drug permeation across cellular barriers and drug exposure to selective cell types. Front. Pharmacol. 9, 27.
Kremsmayr, T., Aljnabi, A., Blanco-Canosa, J.B., Tran, H.N.T., Emidio, N.B., Muttenthaler, M., 2022. On the utility of chemical strategies to improve peptide gut stability. J. Med. Chem. 65, 6191–6206.
Kurrikoff, K., Gestin, M., Langel, U., 2016. Recent *in vivo* advances in cell-penetrating peptide-assisted drug delivery. Expert. Opin. Drug. Deliv. 13, 373–387.
Lai, Z., Yuan, X., Chen, W., Chen, H., Li, B., Bi, Z., Lyu, Y., Shan, A., 2024. Design of proteolytic-resistant antifungal peptides by utilizing minimum D-amino acid ratios. J. Med. Chem. 67, 10891–10905.
Lavecchia, A., Di Giovanni, C., Cerchia, C., Russo, A., Russo, G., Novellino, E., 2013. Discovery of a novel small molecule inhibitor targeting the frataxin/ubiquitin interaction via structure-based virtual screening and bioassays. J. Med. Chem. 56, 2861–2873.
Levental, I., Lyman, E., 2023. Regulation of membrane protein structure and function by their lipid nano-environment. Nat. Rev. Mo.l Cell Biol. 24, 107–122.
Li, P., Roller, P.P., 2002. Cyclization strategies in peptide derived drug design. Curr. Top. Med. Chem. 2, 325–341.
Liu, J., Cabral, H., Mi, P., 2024. Nanocarriers address intracellular barriers for efficient drug delivery, overcoming drug resistance, subcellular targeting and controlled release. Adv. Drug. Deliv. Rev. 207, 115239.
Lucana, M.C., Arruga, Y., Petrachi, E., Roig, A., Lucchi, R., Oller-Salvia, B., 2021. Protease-resistant peptides for targeting and intracellular delivery of therapeutics. Pharmaceutics 13, 2065.
Lutolf, M.P., Radisic, M., Beekman, J., Huh, D.D., Huch, M., Turco, M.Y., Birgani, Z.N.T., Gao, D., Yao, R., Lin, H., Takebe, T., 2024. *In vitro* human cell-based models: what can they do and what are their limitations? Trends. Biotechnol. 42, 1577–1582.
Ma, W., Tang, C., Lai, L., 2005. Specificity of trypsin and chymotrypsin: loop-motion-controlled dynamic correlation as a determinant. Biophys. J. 89, 1183–1193.
Mi, P., Cabral, H., Kataoka, K., 2020. Ligand-installed nanocarriers toward precision therapy. Adv. Mater. 32, e1902604.
Moreno-Vargas, L.M., Prada-Gracia, D., 2024. Exploring the chemical features and biomedical relevance of cell-penetrating peptides. Int. J. Mol. Sci. 26, 59.
Mukherjee, P., Mukhopadhyay, T.K., Mukherjee, M., Roy, P., Ghosh, R., Sardar, P.S., Ghosh, S., 2024. Triplet state spectroscopy reveals involvement of the buried tryptophan residue 310 in glyceraldehyde-3-phosphate dehydrogenase (GAPD) in the interaction with acrylamide. Spectrochim. Acta. A. Mol. Biomol. Spectrosc. 307, 123622.
Nikitovic, D., Kukovyakina, E., Berdiaki, A., Tzanakakis, A., Luss, A., Vlaskina, E., Yagolovich, A., Tsatsakis, A., Kuskov, A., 2024. Enhancing tumor targeted therapy: the role of iRGD peptide in advanced drug delivery systems. Cancers (Basel) 16, 3768.
Parrasia, S., Szabo, I., Zoratti, M., Biasutto, L., 2022. Peptides as pharmacological carriers to the brain: promises, shortcomings and challenges. Mol. Pharm. 19, 3700–3729.
Pecoraro, A., Carotenuto, P., Russo, G., Russo, A., 2019. Ribosomal protein uL3 targets E2F1 and cyclin D1 in cancer cell response to nucleolar stress. Sci. Rep. 9, 15431.
Pei, J., Gao, X., Pan, D., Hua, Y., He, J., Liu, Z., Dang, Y., 2022. Advances in the stability challenges of bioactive peptides and improvement strategies. Curr. Res. Food. Sci. 5, 2162–2170.
Ruseska, I., Zimmer, A., 2020. Internalization mechanisms of cell-penetrating peptides. Beilstein. J. Nanotechnol. 11, 101–123.
Sahni, A., Qian, Z., Pei, D., 2020. Cell-penetrating peptides escape the endosome by inducing vesicle budding and collapse. ACS. Chem. Biol. 15, 2485–2492.
Sarnella, A., Ferrara, Y., Terlizzi, C., Albanese, S., Monti, S., Licenziato, L., Mancini, M., 2024. The chicken embryo: an old but promising model for *In vivo* preclinical research. Biomedicines. 12, 2835.
Sawosz, E., Jaworski, S., Kutwin, M., Hotowy, A., Wierzbicki, M., Grodzik, M., Kurantowicz, N., Strojny, B., Lipinska, L., Chwalibog, A., 2014. Toxicity of pristine graphene in experiments in a chicken embryo model. Int. J. Nanomedicine. 9, 3913–3922.
Sezgin, E., Levental, I., Mayor, S., Eggeling, C., 2017. The mystery of membrane organization: composition, regulation and roles of lipid rafts. Nat. Rev. Mol. Cell. Biol. 18, 361–374.
Strambini, G.B., Gonnelli, M., 2010. Fluorescence quenching of buried trp residues by acrylamide does not require penetration of the protein fold. J. Phys. Chem. B. 114, 1089–1093.
Struck, D.K., Hoekstra, D., Pagano, R.E., 1981. Use of resonance energy transfer to monitor membrane fusion. Biochemistry 20, 4093–4099.
Valiante, S., Falanga, A., Cigliano, L., Iachetta, G., Busiello, R.A., La Marca, V., Galdiero, M., Lombardi, A., Galdiero, S., 2015. Peptide gH625 enters into neuron and astrocyte cell lines and crosses the blood-brain barrier in rats. Int. J. Nanomedicine. 10, 1885–1898.
Vargason, A.M., Anselmo, A.C., Mitragotri, S., 2021. The evolution of commercial drug delivery technologies. Nat. Biomed. Eng. 5, 951–967.
Virgilio, A., Benigno, D., Pecoraro, A., Russo, A., Russo, G., Esposito, V., Galeone, A., 2021. Exploring new potential anticancer activities of the G-quadruplexes formed by [(GTG(2)T(G(3)T)(3)] and its derivatives with an Abasic site replacing single thymidine. Int. J. Mol. Sci. 22, 7040.
Voss, S., Adair, L.D., Achazi, K., Kim, H., Bergemann, S., Bartenschlager, R., New, E.J., Rademann, J., Nitsche, C., 2024. Cell-penetrating peptide-bismuth bicycles. Angew. Chem. Int. Ed. Engl. 63, e202318615.
Vreeke, G.J.C., Vincken, J.P., Wierenga, P.A., 2023. The path of proteolysis by bovine chymotrypsin. Food. Res. Int. 165, 112485.
Walrant, A., Cardon, S., Burlina, F., Sagan, S., 2017. Membrane crossing and membranotropic activity of cell-penetrating peptides: dangerous liaisons? Acc. Chem. Res. 50, 2968–2975.
Wimley, W.C., 2015. Determining the effects of membrane-interacting peptides on membrane integrity. Methods. Mol. Biol. 1324, 89–106.
Wishart, D.S., Sykes, B.D., Richards, F.M., 1991. Simple techniques for the quantification of protein secondary structure by 1H NMR spectroscopy. FEBS Lett 293, 72–80.
Wu, D., Chen, Q., Chen, X., Han, F., Chen, Z., Wang, Y., 2023. The blood-brain barrier: structure, regulation, and drug delivery. Signal. Transduct. Target. Ther. 8, 217.
Wu, K., Kwon, S.H., Zhou, X., Fuller, C., Wang, X., Vadgama, J., Wu, Y., 2024. Overcoming challenges in small-molecule drug bioavailability: a review of key factors and approaches. Int. J. Mol. Sci. 25, 13121.
Wuthrich, K., 1986. NMR of Proteins and Nucleic Acids. Wiley, New York.
Yan, L., Ke, Y., Kan, Y., Lin, D., Yang, J., He, Y., Wu, L., 2020. New insight into enzymatic hydrolysis of peptides with site-specific amino acid D-isomerization. Bioorg. Chem. 105, 104389.
Yang, N.J., Hinner, M.J., 2015. Getting across the cell membrane: an overview for small molecules, peptides, and proteins. Methods Mol. Biol. 1266, 29–53.
Zhang, R., Qin, X., Kong, F., Chen, P., Pan, G., 2019. Improving cellular uptake of therapeutic entities through interaction with components of cell membrane. Drug. Deliv. 26, 328–342.
Zhang, H., Zhang, Y., Zhang, C., Yu, H., Ma, Y., Li, Z., Shi, N., 2023. Recent advances of cell-penetrating peptides and their application as vectors for delivery of peptide and protein-based cargo molecules. Pharmaceutics 15, 2093.
Zhao, Y., Zhang, M., Qiu, S., Wang, J., Peng, J., Zhao, P., Zhu, R., Wang, H., Li, Y., Wang, K., Yan, W., Wang, R., 2016. Antimicrobial activity and stability of the D-amino acid substituted derivatives of antimicrobial peptide polybia-MPI. AMB Express 6, 122.
Zhou, X., Smith, Q.R., Liu, X., 2021. Brain penetrating peptides and peptide-drug conjugates to overcome the blood-brain barrier and target CNS diseases. Wiley Interdiscip. Rev. Nanomed. Nanobiotechnol. 13, e1695.